Inactivation Gating of Kv4 Potassium Channels
Molecular Interactions Involving the Inner Vestibule of the Pore

Henry H. Jerng, Mohammad Shahidullah, and Manuel Covarrubias

From the Department of Pathology, Anatomy and Cell Biology, Jefferson Medical College, Philadelphia, Pennsylvania 19107

ABSTRACT   Kv4 channels represent the main class of brain A-type K^+ channels that operate in the subthreshold range of membrane potentials (Serodio, P., E. Vega-Saenz de Miera, and B. Rudy. 1996. *J. Neurophysiol.* 75:2174–2179), and their function depends critically on inactivation gating. A previous study suggested that the cytoplasmic NH_2- and COOH-terminal domains of Kv4.1 channels act in concert to determine the fast phase of the complex time course of macroscopic inactivation (Jerng, H.H., and M. Covarrubias. 1997. *Biophys. J.* 72:163–174). To investigate the structural basis of slow inactivation gating of these channels, we examined internal residues that may affect the mutually exclusive relationship between inactivation and closed-state blockade by 4-aminopyridine (4-AP) (Campbell, D.L., Y. Qu, R.L. Rasmussen, and H.C. Strauss. 1993. *J. Gen. Physiol.* 101:603–626; Shieh, C.-C., and G.E. Kirsch. 1994. *Biophys. J.* 67:2316–2325). A double mutation V[404,406]I in the distal section of the S6 region of the protein drastically slowed channel inactivation and deactivation, and significantly reduced the blockade by 4-AP. In addition, recovery from inactivation was slightly faster, but the pore properties were not significantly affected. Consistent with a more stable open state and disrupted closed state inactivation, V[404,406]I also caused hyperpolarizing and depolarizing shifts of the peak conductance–voltage curve (∼5 mV) and the prepulse inactivation curve (>10 mV), respectively. By contrast, the analogous mutations (V[556,558]I) in a K^+ channel that undergoes N- and C-type inactivation (Kv1.4) did not affect macroscopic inactivation but dramatically slowed deactivation and recovery from inactivation, and eliminated open-channel blockade by 4-AP. Mutation of a Kv4-specifc residue in the S4–S5 loop (C322S) of Kv4.1 also altered gating and 4-AP sensitivity in a manner that closely resembles the effects of V[404,406]I. However, this mutant did not exhibit disrupted closed state inactivation. A kinetic model that assumes coupling between channel closing and inactivation at depolarized membrane potentials accounts for the results. We propose that components of the pore's internal vestibule control both closing and inactivation in Kv4 K^+ channels.

KEY WORDS: Shal channels • inactivation kinetics • A-type currents • 4-aminopyridine

introduction

Voltage-gated K^+ channels (Kv channels)[1] activate and open upon membrane depolarization. Most Kv channels, however, do not remain open during a sustained depolarization. Instead, they adopt a nonconducting conformation by a process known as inactivation. Kv channels may exhibit multiple mechanisms of inactivation that involve fast and slow processes. A great deal has been learned about the mechanisms of inactivation of *Shaker* K^+ channels. These channels exhibit two clearly distinct forms of inactivation: N- and C-type (Choi et al., 1991). N-type inactivation is fast and involves a "ball and chain"–type mechanism (Armstrong and Bezanilla, 1977), where approximately the first 20 amino acids at the NH_2 terminus of the *Shaker* subunit act as a tethered internal particle capable of blocking the open pore (Hoshi et al., 1990; Demo and Yellen, 1991; Ruppersberg et al., 1991; Murrell-Lagnado and Aldrich, 1993; Tseng-Crank et al., 1993; MacKinnon et al., 1993; Gomez-Lagunas and Armstrong, 1995). The cytoplasmic loop between the S4 and S5 seqments (the S4–S5 loop) contributes to the putative receptor for the inactivation particle in the pore of the channel (Isacoff et al., 1991; Holmgren et al., 1996). C-type inactivation is typically slower than N-type and depends on residues in the pore region (the S5–S6 loop) and the external section of the S6 region (Hoshi et al., 1991; Lopez-Barneo et al., 1993). The rate of C-type inactivation is slower in the absence of N-type inactivation, suggesting that the two processes are coupled (Hoshi et al., 1991; Baukrowitz and Yellen, 1995). A current hypothesis proposes that C-type inactivation involves a rearrangement of the extracellular mouth of the pore resulting from a cooperative conformational change of the channel subunits (Ogielska et al., 1995; Panyi et al., 1995;

[1]*Abbreviations used in this paper:* 4-AP, 4-aminopyridine; G/V, conductance–voltage; Kv channel, voltage-gated K^+ channel.

Liu et al., 1996; Loots and Isacoff, 1998). As a result, C-type–inactivated channels become more permeable to Na$^+$ (Starkus et al., 1997; Kiss, 1999).

Although it is clear that certain non-*Shaker* K$^+$ channels may also undergo inactivation by the N- and C-type mechanisms (Ruppersberg et al., 1991; Rettig et al., 1992; Covarrubias et al., 1994; Smith et al., 1996), in various instances the presence of N- or C-type inactivation has been difficult to recognize (e.g., DeBiasi et al., 1993; Jerng and Covarrubias, 1997; Klemic et al., 1998). Therefore, there is a distinct possibility that other Kv channels may undergo inactivation by processes that are not yet understood. In a previous study, we found that rapid inactivation in Kv4.1 K$^+$ channels (members of the Shal family) depends on the concerted action of the cytoplasmic NH$_2$- and COOH-terminal domains of the channel protein (Jerng and Covarrubias, 1997). This process, however, has little impact on the slower processes that contribute to most of the time course of inactivation. To gain insights into the molecular mechanism of slow inactivation of Kv4.1 K$^+$ channels, we have focused on residues that may contribute to the inner vestibule of the channel.

An important clue about the mechanism of inactivation of Kv4 channels (Kv4.1, Kv4.2, and Kv4.3) originated from previous studies that examined the action of 4-aminopyridine (4-AP) on these channels. 4-AP blocks native Kv4 A-type K$^+$ channels from cardiac tissue and cloned Kv4 K$^+$ channels at an internal site with a keen state dependence. Blockade occurs almost exclusively in the closed state, and can be relieved by channel opening and inactivation (Campbell et al., 1993b; Tseng et al., 1996; Jerng, 1998). 4-AP binding and channel inactivation are mutually exclusive because inactivation cannot occur until 4-AP dissociates, and channel inactivation prevents 4-AP binding. These results suggested that residues contributing to the 4-AP binding might also be involved in controlling inactivation of Kv4 channels at an internal site. Inactivation may physically hinder 4-AP binding, and the sites that control the underlying conformational change may also interact with 4-AP. In the distal section of S6 (a putative component of the inner vestibule of the pore), two critical positions are occupied by valines in most Kv channels (Fig. 1, A and C), and their presence is associated with moderate or high sensitivity to 4-AP. Shab K$^+$ channels (Kv2), which exhibit very low 4-AP sensitivity and inactivate very slowly, appear to be the exception (Shieh and Kirsch, 1994). There, the equivalent positions are occupied by isoleucine. We asked whether V → I mutations at these conserved positions in Kv4.1 (V[404,406]I) could simultaneously reduce 4-AP sensitivity and alter inactivation gating in the presence and absence of the cytoplasmic NH$_2$- and COOH-terminal domains.

In several Kv channels, mutations in the S4–S5 loop

and the cytoplasmic regions of S5 and S6 affect binding of the inactivation particle, single channel conductance, K$^+$ selectivity, and blockade by internal tetraethylammonium, 4-AP, Ba^{2+}, and Mg^{2+} (Isacoff et al., 1991; Kirsch et al., 1993; Slesinger et al., 1993; Lopez et al., 1994; Shieh and Kirsch, 1994; Taglialatela et al., 1994). Therefore, the S4–S5 loop and the cytoplasmic halves of S5 and S6 segments appear to contribute to the permeation pathway at the inner vestibule of Kv channels. We hypothesize that a Kv4-specific cysteine in the S4–S5 loop (C322) also contributes to inactivation gating directly or through an interaction with residues in the distal section of S6. The equivalent position is occupied by serine in other Kv channels (Fig. 1 B). Thus, we also examined the biophysical properties of C322S.

The main effects of the V[404,406]I and C322S mutations in the Kv4.1 K$^+$ channels were: (a) to reduce the sensitivity to 4-AP, and (b) to drastically slow the development of macroscopic inactivation and current deactivation (with little effect on the recovery from inactivation). However, while V[404,406]I also slowed the rate of closed state inactivation, C322S did not. The results suggest novel interactions between channel closing, closed-state inactivation, and blockade by 4-AP, which involve the inner vestibule of the pore. To test whether the distal section of S6 may have a similar function in other A-type channels, we also examined the effect of the homologous mutations in Kv1.4 (V[556,558]I), a mammalian *Shaker* K$^+$ channel that exhibits open-channel blockade by 4-AP (Yao and Tseng, 1994; Rasmusson et al., 1995) and features the N- and C-type inactivation mechanisms (Ruppersberg et al., 1991; Pardo et al., 1992; Tseng-Crank et al., 1993; Rasmusson et al., 1995; Lee et al., 1996). The V[556,558]I mutation in Kv1.4 had little or no effect on the development of macroscopic inactivation, but slowed current deactivation and recovery from inactivation, and eliminated blockade by 4-AP. These results further support the idea of a novel mechanism of inactivation at the inner vestibule of Kv4 K$^+$ channels. The main observations can be modeled by a kinetic scheme assuming that an important pathway of Kv4 inactivation originates from a closed state that precedes channel opening.

materials and methods

Molecular Biology

Wild-type mouse Kv4.1 and human Kv1.4 were maintained in pBluescript II KS (Stratagene Inc.) and pRc/CMV (Invitrogen Corp.), respectively. Dr. Carol Deutsch (University of Pennsylvania, Philadelphia, PA) kindly provided Kv1.4. ΔN71/ΔC158 was generated as described previously (Jerng and Covarrubias, 1997). Point mutations were created using two methods. QuickChange (Stratagene Inc.) was used according to the manufacturer's specifications to obtain V[404,406]I, V[404]I, V[406]I, ΔN71/ΔC158/C322S, and ΔN71/ΔC158/V[404,406]I. In brief, pairs of

A

OUT

S1 S2 S3 S4 S5 P S6

Val⁴⁰⁴ → Val^{404}
Val⁴⁰⁶ → Val^{406}

Cys^{322}

IN

N

C
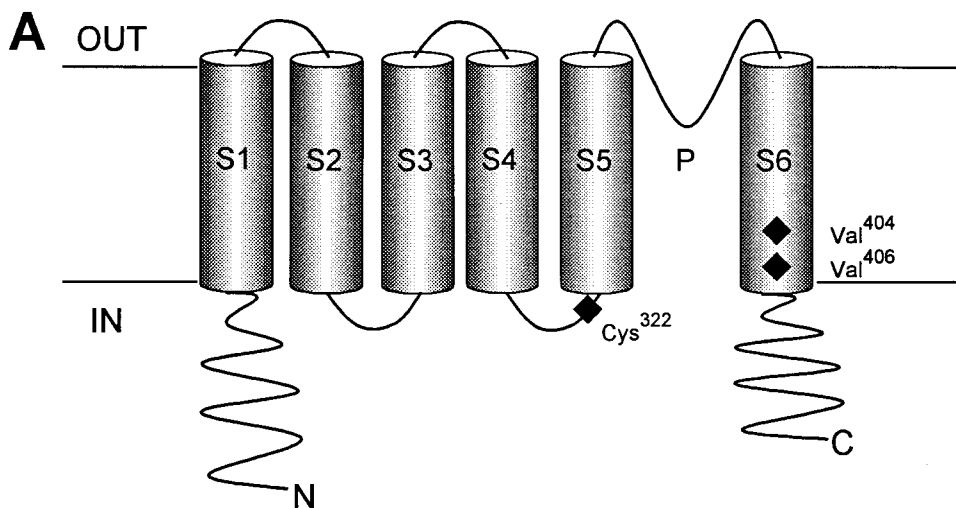
B

```
                         S4                        S5
                        310         320           330
                         *           *  @           *
    mKv4.1    KFSRHSQGLRILGYTLKSCASELGFLLFS
    rKv4.2    ............................
      Shal    .........................V..
  Shaker H4   .L....K..Q...R...ASMR...L.I.F
    rKv1.1    .L....K..Q...Q...ASMR...L.I.F
    rKv1.4    .L....K..Q...H..RASMR...L.I.F
      Shab    .LA...T..QS..F..RNSYK...L.MLF
    rKv2.1    .LA...T..QS..F..RRSYN...L.ILF
      Shaw    .LT...S..K..IQ.FRAS.K..TL.V.F
    rKv3.1    .LT..FV...V..H..RASTN.FLL.IIF
    rKv3.4    .LT..FV...V..H..RASTN.FLL.IIF
```

C

```
                              S6
                       390        400       410
                        *          *  @  @    *
    mKv4.1    STIAGKIFGSICSLSGVLVIALPVPVIVSNFSRIY
    rKv4.2    K..................................
      Shal    E......V.GV........................
  Shaker H4   VGVW...V..L.AIA...T............NYF.
    rKv1.1    V..G...V..L.AIA...T............NYF.
    rKv1.4    I..G...V..L.AIA...T............NYF.
      Shab    T.AL..VI.TV.CIC....V...I.I..N..AEF.
    rKv2.1    K.LL...V.GL.CIA.......I.I..N...EF.
      Shaw    K.YI.MFV.AL.A.A...T............AMY.
    rKv3.1    Q.WS.MLV.AL.A.A...T..M......N..GMY.
    rKv3.4    K.WS.MLV.AL.A.A...T..M......N..GMY.
```

FIGURE 1. Putative K⁺ channel subunit topology and amino acid sequences of the S4–S5 loop and the S6 segment. (A) The folding pattern of the membrane-spanning regions of a voltage-gated K⁺ channel subunit as determined by hydropathy analysis. The residues of interest in this study are C322 in the S4–S5 linker and V404 and V406 in the distal section of the S6 segment (◆, approximate location). (B) Amino acid sequence of the S4–S5 loops from related K⁺ channels (Shal, *Shaker*H4, Shab, and Shaw from *Drosophila*; prefix: m, mouse; r, rat). Relative to Kv4.1, periods indicate identical residues, and the @ symbol marks C322. This residue is Kv4 specific. (C) Amino acid sequence from the same K⁺ channels as in B, covering S6. The symbol representation is the same as in B, with the @ symbols indicating V404 and V406. These residues are found in most subfamilies. The exception is the Shab subfamily, where the equivalent positions are I405 and I407. The residues of interest are highlighted.

mutagenic oligonucleotide primers (Nucleic Acid Facility, Jefferson Cancer Institute) with complementary sequences were used to introduce the desired mutations. The reaction mixture consisted of reaction buffer, DNA template (50 ng), complementary primers (125 ng each), free deoxyribonucleotide mix (2.5 mM, each nucleotide), and *Pyrococcus furiosus* (pfu) DNA polymerase. This mixture was subjected to thermal cycling (95°C, 30 s; 55°C, 1 min; and 68°C, 12–17 min). Over 12–18 cycles (depending on the number of substitutions), the mutagenic oligonucleotide primers annealed to the melted DNA template and by a simple extension process pfu polymerase synthesized the new DNA strands with the intended mutation(s). DpnI (Promega Corp.) was then added to cleave the original DNA template (DpnI cleaves methylated DNA only). Subsequently, the mutated DNA

was electroporated into DH5α cells (GIBCO BRL) and selected colonies were analyzed for the presence of the mutated plasmid. To confirm the phenotype of these mutants, at least two independent clones were examined. C322S and other mutations in the S4–S5 loop were obtained by oligonucleotide-directed mutagenesis using the Altered Sites II in vitro Mutagenesis System (Promega Corp.) as described before (Jerng and Covarrubias, 1997). All mutations were confirmed by automated sequencing (Nucleic Acid Facility). Capped cRNA for expression in *Xenopus* oocytes was produced by in vitro transcription using the Message Machine Kit (Ambion Inc.).

Oocyte Injection and Electrophysiology

Wild-type and mutant Kv4.1 or Kv1.4 cRNAs were injected into defolliculated *Xenopus* oocytes (∼50 ng/cell) using a Nanoject microinjector (Drummond Scientific Co.). Currents were recorded 1–7 d after injection. The two-microelectrode voltage-clamp technique (TEV-200; Dagan Corp.) was used to record whole-oocyte currents. Microelectrodes were filled with 3 M KCl (tip resistance was <1 MΩ). The bath solution contained (mM): 96 NaCl, 2 KCl, 1.8 CaCl$_2$, 1 MgCl$_2$, 5 HEPES, pH 7.4, adjusted with NaOH. In some experiments with low-expressing oocytes, we supplemented the bath solution with 100–500 μM diisothiocyanatostilbene-2,2′-sulfonic acid (DIDS) to block endogenous Ca^{2+}-activated Cl$^-$ conductance and phospholemman-like currents (Jerng and Covarrubias, 1997). Current traces (generally 900-ms depolarizations) were low-pass filtered at 1 kHz (−3 db) and digitized at 500 μs/point. The average voltage offset recorded at the end of an experiment was generally small −0.4 + 2.5 mV, $n = 38$) and was not subtracted from the command voltage. Correction was applied when offset appeared to be greater than 1 SD. The leak current was subtracted off line, assuming ohmic leak or using a P/4 procedure. 4-AP (Sigma Chemical Co.) was dissolved directly in the external bath solution with a reduced concentration of NaCl to maintain normal osmolarity and ionic strength (pH was adjusted to 7.4 with HCl).

Patch-clamp recording was conducted as described before (Chabala et al., 1993) using an Axopatch 200A (Axon Instruments). Patch pipettes were constructed from Corning glass 7052 (Warner Instrument Corp.) and coated with Sylgard elastomer (Dow Corning Co.). Typically, the tip resistance of the recording pipettes in the bath solution (see below) was <1 and 5–30 MΩ for macropatch recording and single channel recording, respectively. The pipette solution (external) was as described above. The bath solution contained (mM): 130 K-aspartate, 10 KCl, 1.8 CaCl$_2$, and 10 HEPES, pH 7.3, adjusted with KOH. Passive leak and capacitive transients from macropatch currents were subtracted on line using a P/4 procedure. For single channel recordings, the passive components of the currents were subtracted using an average of blank sweeps (no single channel currents). Depending on the speed of the current relaxations and the duration of single channel current transitions, the recordings were filtered at 0.5–8 kHz (−3 db, eight-pole Bessel filter; Frequency Devices Inc.) and digitized at 2–40 kHz. Whole-oocyte currents were recorded at 23°C using a temperature-controlled microscope stage (PDMI-2; Medical Systems Corp.). Patch-clamp experiments were recorded at room temperature (22 ± 1°C).

Contrary to the wild-type channels, some biophysical properties of V[404,406]I channels were sensitive to seasonal variation. Most of the experiments reported here were conducted during the Summer and Fall of 1997. Greater variability was apparent when examining the results of experiments conducted ∼3 mo later. Mainly, the parameters affected were the midpoints of the conductance–voltage (G/V) curve and the prepulse inactivation curve, which were more depolarized than the values observed

earlier (∼10 mV in both cases). Consistent with a more depolarized midpoint of prepulse inactivation, closed-state inactivation appeared slower (at least 20 s were necessary to reach a steady state level). Also, the 50% rise time was approximately twofold slower but the tail current relaxations were not significantly affected (see RESULTS).

### Data Acquisition, Analysis, and Model Simulations

Voltage-clamp protocols and data acquisition were controlled by a 586 desktop computer interfaced to a 12-bit A/D converter (Digidata 1200 using a pClamp 6.0; Axon Instruments). Data analysis was conducted using Clampfit (pClamp 6.0; Axon Instruments), Sigmaplot (Jandel Scientific), or Origin (Microcal Software, Inc.). Current relaxations and other time-dependent processes were described assuming a simple exponential function or the sum of exponential terms (Jerng and Covarrubias, 1997). Unless indicated otherwise, all values are expressed as mean ± SD. Model simulations were conducted by determining the initial equilibrium probabilities of occupying a set of states and the characteristic differential equations of the model. For a particular pulse protocol and set of rate constants, this system of equations was solved numerically using Vjump (Fortran program created by user) or SCoP 3.51 (Simulation Resources, Inc.).

results

Point Mutations in the Distal Section of S6 Reduce 4-AP Sensitivity and Dramatically Slow Inactivation of Kv4.1 Channels

The presence of common structural determinants of inactivation and 4-AP binding in Kv4 K$^+$ channels may explain the mutually exclusive interaction between 4-AP and inactivation gating (see INTRODUCTION). To test this hypothesis, we introduced point mutations that were expected to reduce 4-AP sensitivity and studied their effects on inactivation gating. A double mutant V[404,406]I was investigated because previous findings reported that isoleucines at the equivalent positions in Kv2.1 conferred low 4-AP sensitivity (Shieh and Kirsch, 1994). As expected, V[404,406]I channels exhibited a significantly reduced blockade by 4-AP. At 20 mM, 4-AP blocked ∼17% of the mutant peak current, compared with ∼55% of the wild-type peak current (Table I). In addition, the kinetic properties of the Kv4.1 current were dramatically affected (Figs. 2–4, and Table I).

Cell-attached macropatch recordings of wild-type Kv4.1 macroscopic currents showed a rapid rising phase and a decaying phase, nearly identical to those observed from two-electrode voltage-clamp recordings (Fig. 2 A; Jerng and Covarrubias, 1997). Inactivation of these currents was almost complete by the end of the 900-ms depolarization. By contrast, the currents expressed by V[404,406]I decayed at a much slower rate at all voltages and failed to inactivate by the end of the pulse (Fig. 2, B and C). The degree of inactivation was determined by the ratio $I_{(450\ ms)}/I_{peak}$. Wild-type and mutant channels exhibited 10-fold difference in the de-
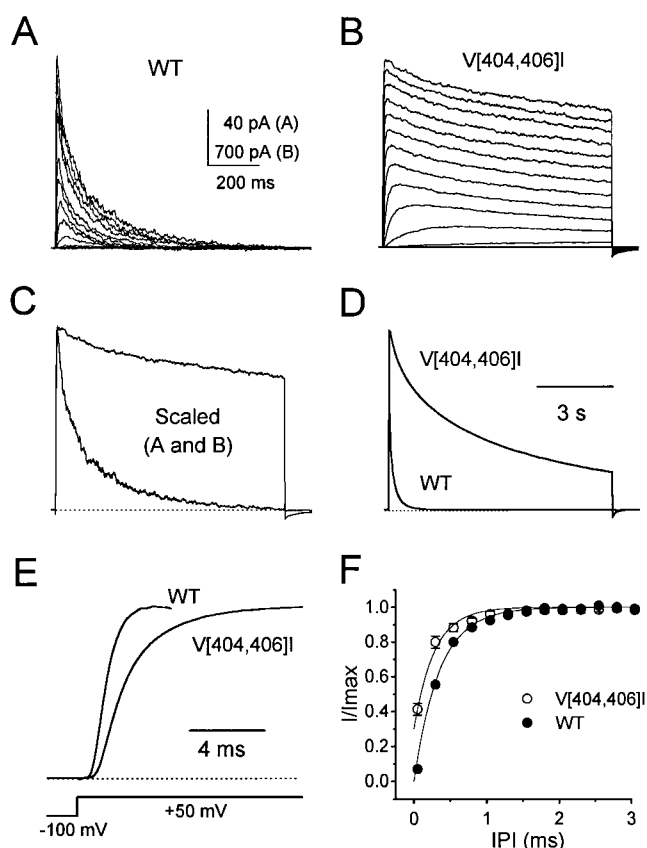
FIGURE 2. Macroscopic currents recorded from *Xenopus* oocytes expressing Kv4.1 K$^+$ channels. (A) Wild-type macropatch outward currents evoked by 900-ms step depolarizations from a holding potential of -100 mV to test potentials from -80 to $+60$ mV in 10-mV increments (the displayed currents are the average of three consecutive runs). The interpulse interval was 5 s. (B) V[404,406]I outward currents evoked as described in A. Recordings in A and B were obtained in the cell-attached configuration of the patch-clamp method (MATERIALS AND METHODS). (C) Comparison of normalized currents at $+60$ mV from A and B. (D) Normalized whole-oocyte outward currents evoked by a 9-s step depolarization to $+50$ mV from a holding potential of -100 mV. (E) The rising phase of the macroscopic currents evoked as described in C. For comparison, the currents are shown normalized. These currents were low-pass filtered at 2.5 kHz and digitized at <100 μs/point (the displayed currents are the average of 15 consecutive runs). (F) The time course of recovery from inactivation at -100 mV. This experiment recorded whole-oocyte currents elicited by a double pulse protocol. From a holding potential of -100 mV, a step depolarization to $+40$ mV evoked the control current and allowed inactivation to occur (500 ms for wild-type channels and 9 s for mutant channels). After a variable interval (interpulse interval [IPI]) at the same holding potential, a second 250-ms pulse was delivered to test for the recovery of the current. The interepisode interval was 5 s. The peak value of the current evoked by the second pulse is divided by that of the current evoked by the first pulse. The graph shows this ratio as a function of the IPI. The open symbols and bars represent the means ± SD of three experiments. To compare the same interpulse intervals, the graph shows a single experiment from wild type (for additional results see Table I). These data were described assuming an exponential rise (solid lines). The best-fit estimates of the time constants were 343 and 265 ms for wild-type and mutant channels, respectively.

gree of inactivation at $+50$ mV (wild type: $0.08 + 0.02$, $n = 5$; V[404,406]I: $0.79 + 0.04$, $n = 9$). Over a prolonged depolarization, however, V[404,406]I mutant channels continued to inactivate (Fig. 2 D). A double exponential fit to the decay of these currents (at $+50$ mV) showed that, relative to the wild-type currents, the estimated steady state level of the current increased approximately fourfold (Table I). This increase suggests the possibility that the inactivated state was destabilized at positive voltages, and, consistent with this idea, the V[404,406]I channels exhibited moderately accelerated recovery from inactivation at -100 mV (Fig. 2 F, and Table I). Because the V[404,406]I channels inactivate at a very slow rate, a larger fraction of channels will continue to open over a longer period of time after the onset of a depolarization. This fraction corresponds to those channels that were yet to open before inactivation occurred in wild-type channels. In agreement with this idea, we found that the rising phase of the V[404,406]I currents appeared significantly slower when compared with that of wild type (Fig. 2 E). The 50% rise time of current activation at $+50$ mV was increased by ~50% (Table I), but the activation delay (Schoppa and Sigworth, 1998) was not significantly affected (0.97 ± 0.3 and 1.03 ± 0.13 ms for wild type and mutant, respectively, $n = 6$; see DISCUSSION). Overall, these experiments demonstrated that V[404,406]I simultaneously inhibits inactivation and closed-state block by 4-AP, suggesting that the mutated residues are involved in the mechanism that underlies the mutually exclusive interaction between inactivation and 4-AP binding in Kv4 K$^+$ channels.

We also investigated whether both mutations were necessary to produce the changes described above. Qualitatively, the single mutant V406I exhibited reduced blockade by 4-AP and biophysical properties that were similar to those of the double mutant (Table I). The main difference was that the V406I mutant channels exhibited a less dramatic effect on inactivation. The ratio $I_{(450 ms)}/I_{peak}$ for V406I was 0.62 ± 0.04 ($n = 4$), compared with $0.79 + 0.04$ ($n = 9$) for V[404,406]I. Yet the inhibition of the peak current by 4-AP was comparable between the single and double mutants (Table I). The V404I mutant produced nonfunctional channels (two independent clones and three separate batches of oocytes). Because the main difference between V[404,406]I and V406I was the degree of inactivation, we inferred that V404 mainly contributes to inactivation or that the double mutation is necessary to affect inactivation (see below).

V[404,406]I Mutations Affect Gating without Affecting the Permeation Properties

The state dependence of 4-AP blockade indicates that channel gating may dictate 4-AP action. Therefore, we
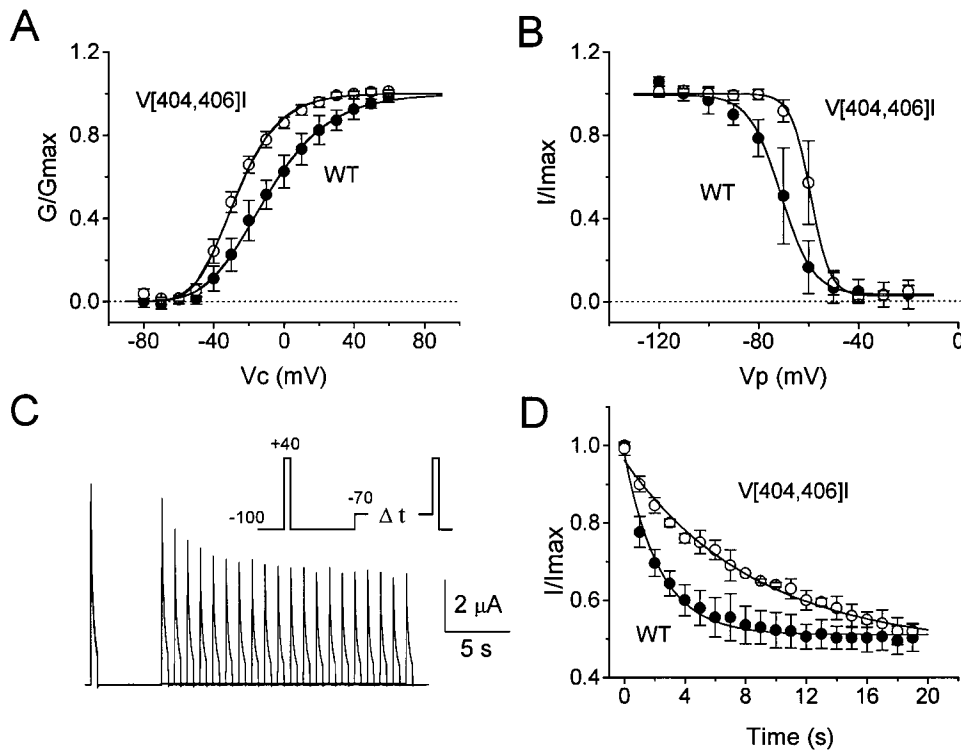
645   Jerng et al.

FIGURE 3. Activation and inactivation properties of macroscopic Kv4.1 currents. (A) The peak G/V relation. The experiments were conducted as described in Fig. 2 (A and B). The peak chord conductance (G) was calculated according to this relation: $G = I_p/(V_c - V_r)$, where I_p is the peak current, V_c is the command voltage (from -80 to $+60$ mV), and V_r is the reversal potential of the current (-95 mV). The peak G/V relation was described assuming a fourth order Boltzmann distribution (Zagotta et al., 1994). For comparison and display, G is divided by G_{max} (the estimated maximal conductance) and plotted against the membrane potential (command voltage). The symbols and bars represent the means $\pm$ SD of nine and seven patches from oocytes expressing wild-type and mutant channels, respectively. The solid lines represent the best-fit fourth-order Boltzmann distributions. The best-fit parameters were: $V_{0.5} = -47$ mV and slope factor $= 22$ mV/e-fold, for the wild-type channels; and $V_{0.5} = -53$ mV and slope factor $= 15$ mV/e-fold, for the mutant channels. (B) Prepulse inactivation curves. The prepulse inactivation protocol consisted of a sequence of two pulses: a 10-s prepulse that was varied between -120 and -10 mV in 10-mV increments and a 250-ms test pulse to $+40$ mV. The holding potential during the interepisode interval (5 s) was -100 mV. The peak of the current evoked by the test pulse was plotted against the prepulse voltage. This relation was described assuming a Boltzmann distribution. For comparison and display, I_p is divided by I_{max} (the maximal control current) and plotted against the prepulse potential. The symbols and bars represent the means $\pm$ SD of five and seven patches from oocytes expressing wild-type and mutant channels, respectively. The solid lines represent the best-fit Boltzmann distributions. The best-fit parameters were: $V_{0.5} = -71$ mV and slope factor $= 6$ mV/e-fold, for the wild-type channels; and $V_{0.5} = -59$ mV and slope factor $= 3.5$ mV/e-fold, for the mutant channels. (C) The time course of prepulse inactivation of wild-type channels at -70 mV. The pulse sequence is shown in the inset. From a holding potential of -100 mV a control 500-ms pulse to $+40$ mV was delivered to obtain the control current. This pulse was followed by a 5-s interval at -100 mV (to recover from inactivation that developed during the first pulse). Then, the membrane was held for a variable interval at a prepulse potential ($\sim V_{0.5}$ of prepulse inactivation) before delivering a 500-ms test pulse to $+40$ mV. The interepisode interval was 5 s. (D) Comparison of the time courses of prepulse inactivation from wild-type and V[404,406]I channels at their corresponding midpoints voltages of prepulse inactivation. Graph displays the relation between the normalized current (I/I_{max}) and the duration of the prepulse. Symbols and bars represent the means $\pm$ SD (wild-type: $n = 3$; V[404,406]I: $n = 4$). The data were described assuming an exponential decay (solid lines). The best-fit estimates of the time constants were 2.3 and 6.7 s for wild-type and mutant channels, respectively.

asked whether the reduced 4-AP sensitivity and slowed inactivation of the V[404,406]I mutant were associated with changes in voltage-dependent gating (Fig. 3). The peak G/V relationships for both wild type and mutant were well described assuming fourth-order Boltzmann distributions (Fig. 3 A; Zagotta et al., 1994). Relative to the wild type, the peak G/V relationship of the V[404,406]I mutant showed a hyperpolarizing shift of ~6 mV in the midpoint potential for activation of one subunit and a reduced slope factor (Fig. 3 A, and Table I). The midpoint potential of prepulse inactivation exhibited a depolarizing shift of ~10 mV and the slope factor was also reduced (Fig. 3 B, and Table I). These results suggested that the mutations had caused a rela-

tive stabilization of the open state and disrupted inactivation at negative voltages. Consistent with this idea, closed-state inactivation of the V[404,406]I channels occurred at a significantly slower rate (Fig. 3, C and D). Interestingly, the V406I channels, which also exhibited slow inactivation at positive potentials, did not show altered closed-state inactivation. As suggested above, V404I in the double mutant is necessary to slow closed-state inactivation at negative voltages. V406I could slow inactivation indirectly by favoring the open state. In such a case, the relative occupancy of an inactivation-permissive closed state that precedes channel opening decreases and the apparent rate of macroscopic inactivation decreases too (see DISCUSSION). To extract more
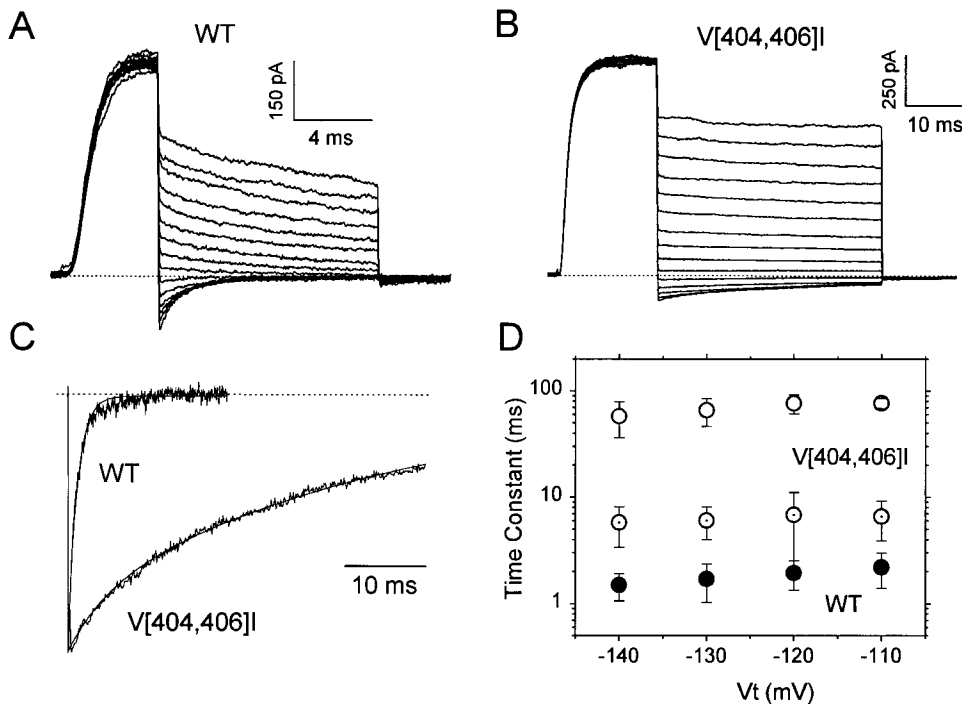
FIGURE 4. Deactivation kinetics of Kv4.1 K$^+$ currents. (A) Wild-type tail currents. After a pulse to +50 mV to activate the current, the membrane was repolarized to membrane potentials between −140 and 0 mV in 10-mV increments. The interepisode interval was 5 s. (B) V[404,406]I tail currents. Currents evoked as described for A. (C) Scaled and superimposed tail currents from A and B at −140 mV. The thin solid lines through the traces are the best fit exponential (wild type) or biexponential curves (V[404,406]I). The estimated time constants were 1.2 ms for wild-type, and 5 (19%) and 41 (81%) ms for V[404,406]I. The numbers in parenthesis are the relative weights of the exponential terms. (D) Time constants of the tail current relaxations as a function of membrane potential. The dotted symbols represent the fast time constants and the open symbols represent the slow time constants.

direct information about the stability of the open state, we examined channel deactivation at hyperpolarized membrane potentials.

Deactivation rates and 4-AP affinities are correlated in Kv channels (Shieh and Kirsch, 1994). This is consistent with observations showing that channel opening influences 4-AP binding in Kv4 open channels (Campbell et al., 1993b; Tseng et al., 1996; Jerng, 1998). Accordingly, V[404,406]I channels, which feature reduced blockade by 4-AP (Table I), also exhibited drastically slower tail currents (Fig. 4, A–C). Wild-type tail currents were well described assuming an exponential relaxation, but a good description of the mutant tail currents required the sum of two exponential terms. In both cases, however, the resulting time constants showed little voltage dependence between −140 and −100 mV (Fig. 4 D). The slow time constant (∼50 ms) dominated the time course of the tail current (∼70%). Relative to the deactivation time constant of wild type, the fast and slow time constants of deactivation of the mutant tail currents at −140 mV were ∼4- and ∼40-fold slower, respectively (Fig. 4, and Table I).

Earlier studies have shown that mutations in the S6 region alter the single channel conductance of certain Kv channels (Lopez et al., 1994; Taglialatela et al., 1994). Because the V[404,406]I mutations are located near the end of the S6 segment, we examined the single channel properties of the wild-type channel and the

V[404,406]I mutant channel. Fig. 5, A and C, shows sets of six consecutive single channel traces evoked by 900-ms step depolarizations to +50 mV from a holding potential of −100 mV and the corresponding ensemble averages (cell-attached patches). The wild-type channels exhibited rapid flickering between the closed and open levels before inactivating. Additional noise was apparent when these channels seemed to fluctuate between the fully open level and subconductance levels (Fig. 5 A, third, fourth, and sixth traces). This complex single channel behavior produced an ensemble average trace that closely matches rapidly inactivating macroscopic currents recorded from macropatches or whole oocytes. Single V[404,406]I channels produced a significantly more stable open level and do not seem to inactivate significantly because channels frequently reopen during the depolarizing pulse (Fig. 5 C; see DISCUSSION). Occasionally, a subconductance level was clearly apparent (Fig. 5 C, first trace), and although the last trace suggests a retarded latency to the first opening this change was not consistently observed (see above for the estimation of activation delay). The average open time of well-resolved full openings was computed to estimate the relative change in the apparent open time between wild-type and V[404,406]I channels. The resulting values were 8.2 ± 3.1 ms (n = 5 patches) and 21.9 ± 3.7 ms (n = 7 patches) for wild-type and mutant channels, respectively (because only well-resolved open-

Properties of Wild-Type and Mutant Kv4.1 Currents

	Wild type	V[404,406]I	V[406]I	C322S	ΔN71/ΔC158 V[404,406]I	ΔN71/ΔC158 C322S
G/V relation*						
$V_{0.5}$ (mV)	−47 ± 4.8	−53.1 ± 2.6	−53.6 ± 4.2	−53.5 ± 4.4	−45.1 ± 2.2	−47.2
S (mV)	22.1 ± 1.7	15.3 ± 1.3	22.4 ± 1.42	23 ± 0	23.5 ± 4.7	20.8
	(n = 9)	(n = 7)	(n = 4)	(n = 4)	(n = 4)	(n = 2)
Prepulse inactivation‡						
$V_{0.5}$ (mV)	−69.0 ± 2.0	−59.3 ± 3.2	−68.3 ± 0.8	−67.0 ± 0.6	−43.4 ± 2.1	−56.1 ± 4.6
S (mV)	5.0 ± 0.4	3.5 ± 0.4	5.0 ± 0.4	4.0 ± 0.2	5.8 ± 0.6	6.3 ± 0.7
	(n = 6)	(n = 5)	(n = 3)	(n = 3)	(n = 6)	(n = 3)
Onset of inactivation§						
τ-1 (ms)	18 ± 3	1257 ± 333	512 ± 126	92.0 ± 5.4	781 ± 99	407 ± 31
τ-2 (ms)	77 ± 11	7782 ± 791	2981 ± 511	889 ± 281	7395 ± 623	3349 ± 905
τ-3 (ms)	273 ± 28			5560 ± 1420		
W-1	0.19 ± 0.04	0.30 ± 0.04	0.33 ± 0.06	0.23 ± 0.14	0.27 ± 0.05	0.36 ± 0.06
W-2	0.35 ± 0.03	0.61 ± 0.01	0.60 ± 0.05	0.16 ± 0.02	0.60 ± 0.03	0.58 ± 0.05
W-3	0.44 ± 0.05			0.53 ± 0.13		
W-ss	0.02 ± 0.01	0.08 ± 0.04	0.07 ± 0.02	0.08 ± 0.03	0.13 ± 0.04	0.06 ± 0.0
	(n = 11)	(n = 5)	(n = 3)	(n = 5)	(n = 3)	(n = 3)
Rise time‖						
$T_{50\%}$ (ms)	1.5 ± 0.4	2.2 ± 0.4	ND	3.4 ± 0.8	ND	ND
	(n = 6)	(n = 6)		(n = 5)		
Deactivation¶						
τ (ms)	1.5 ± 0.42	58 ± 22	ND	14 ± 5	38.0 ± 2.0	ND
	(n = 6)	(n = 5)		(n = 5)	(n = 4)	
Closed-state inactivation**						
τ (ms)	2.2 ± 0.7	7.8 ± 0.9	ND	2.8 ± 0.9	ND	ND
	(n = 3)	(n = 3)		(n = 3)		
Recovery from inactivation‡‡						
τ (ms)	362 ± 58	300 ± 30	332 ± 146	316 ± 46	373 ± 91	255 ± 53
	(n = 4)	(n = 3)	(n = 3)	(n = 4)	(n = 4)	(n = 3)
Single channel conductance§§						
(pS)	5.1 ± 0.7	5.8 ± 0.7	ND	9.4 ± 0.2	ND	ND
	(n = 3)	(n = 4)		(n = 3)		
Reversal potential‖‖						
(mV)	−95.0 ± 3.7	−93 ± 3.8	ND	−85 ± 2.4	ND	ND
	(n = 7)	(n = 7)		(n = 7)		
Block by 4-AP¶¶						
percent inhibition	54.0 ± 3.0	17.0 ± 16.0	23.0 ± 3.0	33.0 ± 6	ND	ND
	(n = 6)	(n = 7)	(n = 3)	(n = 4)		

*The peak G/V curve was described assuming a fourth order Boltzmann function (Fig. 3). $V_{0.5}$ is the midpoint voltage for the activation of one subunit, and S is the slope factor (mV/e-fold). S for C322S was fixed. ‡The prepulse inactivation curve was described assuming a simple Boltzmann distribution (Fig. 3). $V_{0.5}$ is the midpoint voltage, and S is the slope factor (mV/e-fold). §The decay of whole-oocyte currents at +50 mV was described assuming the sum exponential terms. τ-n and W-n represent the time constants and the corresponding relative weights. W-ss is the relative weight of the steady state current. ‖This parameter was estimated by determining the time needed to reach 50% of the peak current at +50 mV. ¶The time course of the tail current at −140 mV was described assuming an exponential relaxation for wild type or the sum of two exponential terms for the mutants. The value shown here is the time constant of the dominant component representing ~70% of the fitted curve (Fig. 4). **This value was obtained as described in Fig. 3 at a prepulse potential that corresponds approximately to the midpoint of prepulse inactivation. ‡‡The time course of recovery from inactivation at −100 mV was described assuming an exponential rise. §§This value was obtained from the analysis of unitary currents as described in Fig. 5. ‖‖Values were estimated from the instantaneous current–voltage relationships in the presence of 2 mM K$^+$ in the bath. ¶¶Inhibition of the peak current by 20 mM 4-AP was estimated at +50 mV.

ings were examined, the apparent open times are over-estimated). The increase in the apparent open time was qualitatively consistent with the slow deactivation of the V[404,406]I channels at hyperpolarized membrane potentials, and the ensemble average trace closely matches slowly inactivating macroscopic currents recorded from macropatches or whole oocytes. These results indicated that the recorded single channel activity
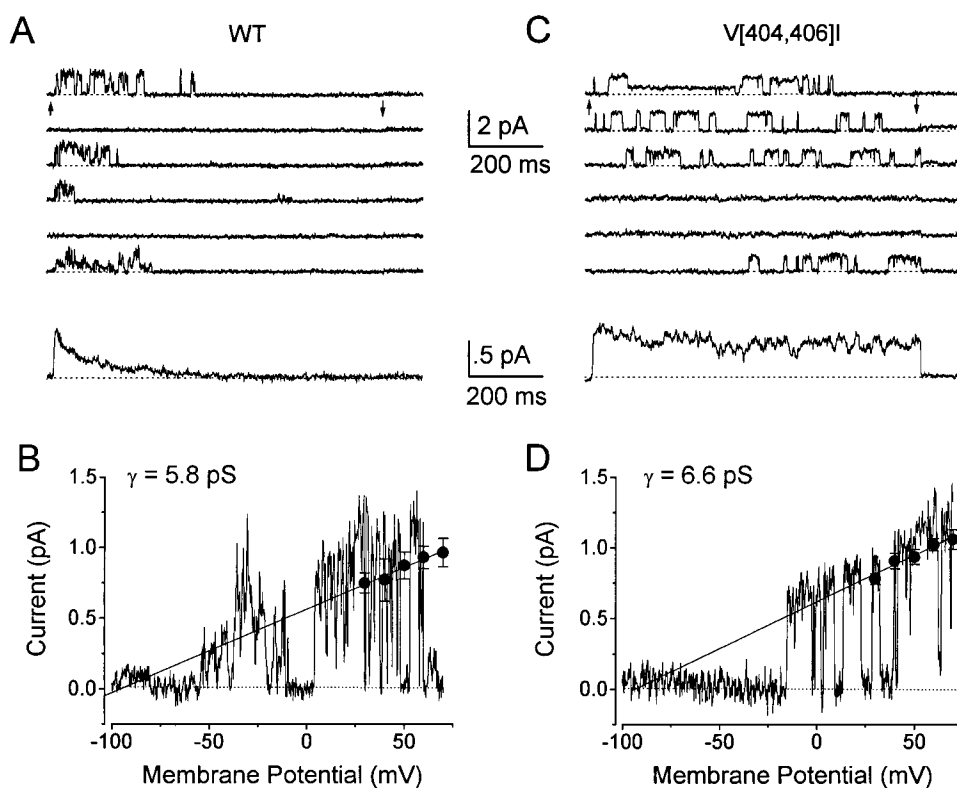
FIGURE 5. Kv4.1 single channel currents. (A and C) Consecutive single channel traces evoked by a step depolarization to +50 mV from a holding potential of −100 mV. The dotted line represents the closed level, and the arrows indicate the beginning and end of the depolarizing pulse. Note rapid flickering and unresolved openings in the wild-type traces, and a more stable open state in the mutant traces. A clear sublevel is resolved in the first mutant trace. The excessively prolonged latency to the first opening in the last mutant trace was not consistently observed (see RESULTS). The corresponding ensemble average currents ($n = 64$ traces) are displayed in the lower part of A and C. All recordings were obtained in the cell-attached configuration. (B and D) The single channel current–voltage relations of Kv4.1 channels. Two methods were used to measure the unitary conductance (γ): (a) by ramping the membrane potential between −100 and +70 mV or (b) by determining the mean unitary current (from amplitude histograms) at various membrane potentials (+30, +40, +50, +60, and +70 mV). Because of rapid flickering and the presence of apparent subconductance levels in the recordings from wild-type channels, only well-resolved full openings were considered in this analysis (note that the mean unitary amplitudes appear slightly underestimated). The solid lines across the currents and the symbols are linear regression fits to the mean values of the unitary currents. Symbols and bars represent the mean ± SD ($n = 3$ and 4 patches in B and D, respectively).

represents gating of the channels under study. Therefore, the single channel records were analyzed further to test whether V[404,406]I affected the single channel conductance.

Two different experimental protocols were used to estimate the single channel conductance. In one, the membrane potential was ramped between −100 and +70 mV. Single channel currents evoked during this voltage ramp are shown in Fig. 5, B and D from patches expressing wild-type and V[404,406]I channels, respectively. In the other, the mean amplitude of discrete single channel openings was estimated from amplitude histograms at different membrane potentials (+30, +40, +50, +60, and +70; Fig. 5, B and D, ●). Clearly, both protocols gave similar results. The estimated slope conductances were 5.1 ± 0.7 pS ($n = 3$ patches) and 5.8 ± 0.7 pS ($n = 4$ patches), for wild-type and mutant channels, respectively. Thus, V[404,406]I did not significantly affect the unitary conductance of Kv4.1 K$^+$ channels. The reversal potentials of wild-type and mutant tail currents in normal external solution (2 mM K$^+$) were also similar (approximately −93 mV; Table I).

Furthermore, the relation between the reversal potential and the concentration of external K$^+$ (substituting Na$^+$ for K$^+$) was examined to verify that the P_{Na}/P_K was not affected by the mutation. The slopes of these relations were nearly identical (58.7 and 57.6 mV/10-fold change in the concentration of external K$^+$ for the wild-type and the V[404,406]I currents, respectively; data not shown). Therefore, V404 and V406 in Kv4.1 K$^+$ channels do not appear to be critical in determining ion permeation and K$^+$ selectivity.

The Effects of V[404,406]I on Current Inactivation and Deactivation Can Be Mimicked by a Mutation at a Unique Site in the S4–S5 Loop

The S4–S5 loop is thought to be an important component of the gating machinery of Kv channels (McCormack et al., 1991, 1993). In addition, the S4–S5 loop appears to contribute to the receptor of the inactivation particle (Isacoff et al., 1991; Holmgren et al., 1996) and ion permeation (Slesinger et al., 1993). Presumably, the S4–S5 loop could play similar roles in Kv4

K$^+$ channels, but that has not been directly investigated. In particular, it is intriguing that position 322 in Kv4.1 (or the equivalent position in all Shal K$^+$ channels) is occupied by cysteine, whereas in other Kv channel subunits the equivalent position is occupied by serine (Fig. 1 B). Mutation of this serine to cysteine in *Shaker* B K$^+$ channels (S392C) destabilizes the inactivated state (Isacoff et al., 1991), probably by affecting the interactions of the S4–S5 loop with the inactivation particle. Thus, because macroscopic inactivation of *Shaker* B K$^+$ channels is much faster than that of Kv4 K$^+$ channels, we had hypothesized that the reverse substitution in Kv4.1 (C322S) could favor inactivation. By contrast, C322S channels exhibit slower macroscopic inactivation (Fig. 6, A and B) and deactivation kinetics (Fig. 6 C, and Table I). The degree of inactivation [$I_{(450\ ms)}$/I_{peak}] at +50 mV is 0.69 ± 0.03 ($n = 6$). Compared with wild-type currents, this figure is approximately eightfold larger. When the current was evoked by a long depolarization (+50 mV, 10 s), there was little or no current remaining by the end of the pulse (Fig. 6 B). The 50% rise time at +50 mV was also slowed by an approximately twofold (1.7 ± 0.3 and 3.4 ± 0.8 ms for wild type ($n = 5$) and mutant ($n = 5$), respectively; Fig. 6 B, inset) and the activation delay was modestly increased (0.97 ± 0.3 and 1.4 ± 0.3 ms for wild type ($n = 6$) and mutant ($n = 5$),

respectively). Tail currents at −140 mV were best described assuming the sum of two exponential terms (Fig. 6 C and legend), with the slow component ($\tau = 13.9 \pm 4$ ms, $n = 5$) dominating the time course of the tail current (~60%). These results are not consistent with the idea that C322 in Kv4.1 and S392 in *Shaker* B play equivalent functions. Interestingly, however, the kinetics of macroscopic activation and inactivation, recovery from inactivation and deactivation of C322S, V[404,406]I, and V406I are similar (Table I). Like the V406I mutant, the prepulse inactivation curve and the peak G/V relation of C322S were only modestly affected (Table I). Also, closed-state inactivation remained unchanged (Fig. 6 D). Notably, however, the blockade of C322S channels by 4-AP was also reduced (Table I). The single channel conductance is one of the most significant differences between the V[404,406]I and C322S mutant channels. The latter mutant roughly doubled the single channel conductance (Table I), a result that is consistent with a contribution of the S4–S5 loop to the ion permeation pathway (Slesinger et al., 1993).

The ability C322S to mimic the inactivation gating properties of V[404,406]I and V406I suggests that two regions that are thought to form the inner vestibule of Kv channels (the S4–S5 loop and the distal section of S6) may in a unique way contribute to inactivation gat-
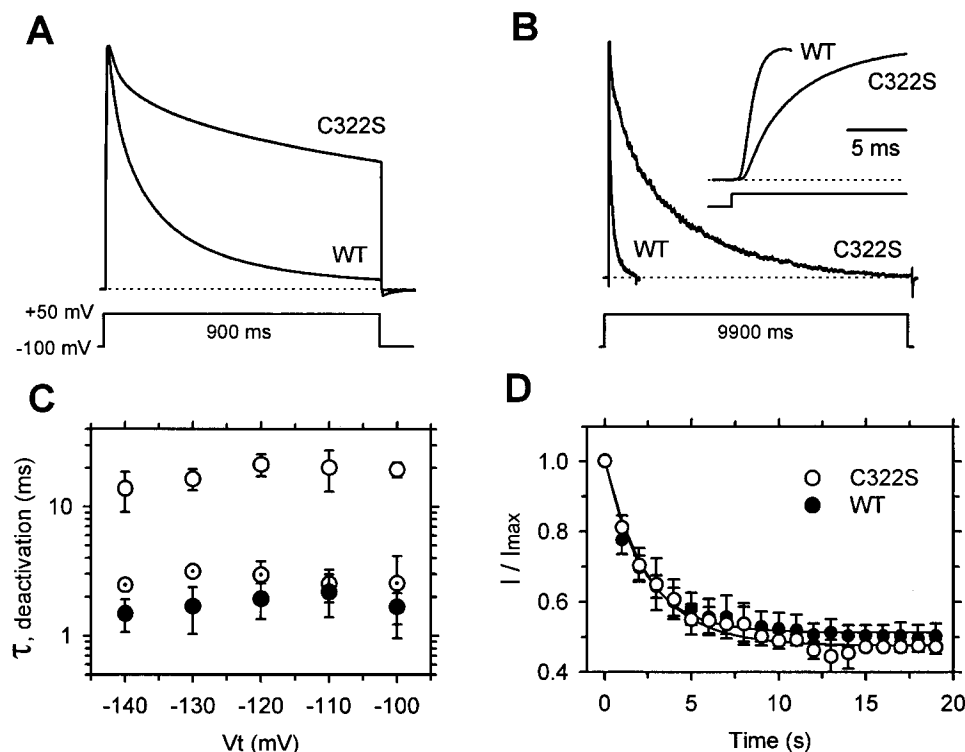

FIGURE 6. Macroscopic properties of C322S channels. (A) Whole-oocyte outward currents evoked by a 900-ms step depolarization to +50 mV from a holding potential of −100 mV. (B) Macropatch outward currents evoked by a 9.9-s step depolarization to +50 mV from a holding potential of −100 mV (C322S only). Mutant and wild-type currents in A and B are shown normalized. The inset shows the rising phase of the currents at +50 mV. The dotted lines in A and B represent the zero current level. (C) Time constants of tail current relaxations. The experiments were conducted and analyzed as described in Fig. 4. The mutant current relaxations were best described assuming the sum of two exponential terms (open and dotted symbols). The wild-type values are replotted from Fig. 4. Symbols and bars represent the mean ± SD (C322S, $n = 6$). (D) Time course of prepulse inactivation. This experiment was conducted and analyzed as described in Fig. 3. For C322S channels, the prepulse potential was −68 mV. The time course corresponding to C322S channels (open symbols) was described assuming an exponential decay ($\tau = 2.6$ s). The data for wild type are replotted from Fig. 3. Symbols and bars represent the mean ± SD (C322S, $n = 3$).

ing in Kv4 K$^+$ channels. This idea is particularly significant in light of the distinct effects of similar mutations in *Shaker* K$^+$ channels (see below). One of the most striking effects of the mutations studied here was the dramatic slowing of deactivation, which in all cases is associated with slow current inactivation (Figs. 4 and 6, and Table I). This relationship is the key to the mechanism of inactivation of Kv4 channels (see DISCUSSION).

V[404,406]I and C322S Introduce Slower Inactivation in the Absence of the NH$_2$- and COOH-terminal Domains

The cytoplasmic NH$_2$- and COOH-terminal domains are necessary to maintain the fast inactivation process (Jerng and Covarrubias, 1997). In the absence of most of the terminal domains, slower inactivation processes remained relatively unchanged (Fig. 7). Thus, there is little or no interaction between the fast and slow processes of inactivation. To examine whether the slow inactivation processes are affected by the S6 and S4–S5 mutations in the absence of the termini, we introduced the V[404,406]I and C322S mutations into a previously studied double deletion mutant (ΔN71/ΔC158 = Δ2–71/Δ494–651; Jerng and Covarrubias, 1997). The main effect of the deletion alone is to eliminate the fast phase of macroscopic inactivation observed at positive membrane potentials (Fig. 7). ΔN71/ΔC158/V[404,406]I dramatically slowed the rising and decaying phases of the current (Fig. 7 A). ΔN71/ΔC158/C322S also slowed macroscopic inactivation and the rising phase but to a lesser extent than ΔN71/ΔC158/V[404,406]I (Fig. 7 B). These observations are qualitatively in agreement with observations made in the presence of the termini (Figs. 2 and 6, and Table I), including the fact that ΔN71/ΔC158/V[404,406]I and ΔN71/ΔC158/C322S continued to inactivate over a period of 9 s (not shown). These results showed that independently of the termini, V404, V406, and C322 help to control inactivation in Kv4 K$^+$ channels. Thus, it is unlikely that the main function of these residues is to contribute to a docking site for a putative cytoplasmic inactivation gate in these channels.

The Distal Section of S6 Controls Gating and 4-AP Binding, but Does Not Affect the Development of Inactivation in a Shaker A-type K$^+$ Channel

Further support for a distinct form of inactivation in Kv4 channels can be found by examining Kv channels that undergo inactivation mainly coupled to channel opening (Hoshi et al., 1990, 1991; Zagotta and Aldrich, 1990; Ruppersberg et al., 1991; Tseng-Crank et al., 1993; Ayer and Sigworth, 1997). In such a case, how does a change in deactivation kinetics affect inactivation gating? We hypothesized that, by contrast to V[404,406]I in Kv4.1, the equivalent mutation in Kv1.4 (V[556,558]I) may not slow the development of macroscopic inactivation, but significantly slow current deactivation and recovery from inactivation. This result is expected because K$^+$ channels of this kind pass through the open state when they recover from inactivation (Demo and Yellen, 1991; Ruppersberg et al., 1991), and the distal section of S6 influences gating (Liu et al., 1997). Both the wild-type and mutant Kv1.4 channels expressed nearly identical outward currents that rapidly activate and inactivate (Fig. 8 A). The decay of these currents is well described assuming a biexponential relaxation (Table II) with time constants that are voltage independent at positive membrane potentials (not shown). As predicted, the V[556,558]I mutation slows the kinetics of deactivation and recovery from inactivation (Fig. 8, B and C) but does not significantly alter the development of macroscopic inactivation (Table II). The time constants of deactivation (at -140 mV) and recovery from inactivation (at -100 mV) increased 10- and 5-fold, respectively (Table II). This result agrees with the hypothesis because channel closing is rate limiting when the channels recover from inactivation passing through the open state (a direct consequence of inactivation mainly coupled to channel opening). The V[556,558]I mutation also destabilizes voltage-dependent activation of Kv1.4 K$^+$ channels because the peak G/V relation and the prepulse inactivation curve exhibit a depolarizing shift of $\sim$10 mV (Ta-

A

ΔN71/ΔC158
V404I/V406I

ΔN71/ΔC158

WT

900 ms

+50 mV

-100 mV

B

ΔN71/ΔC158
C322S

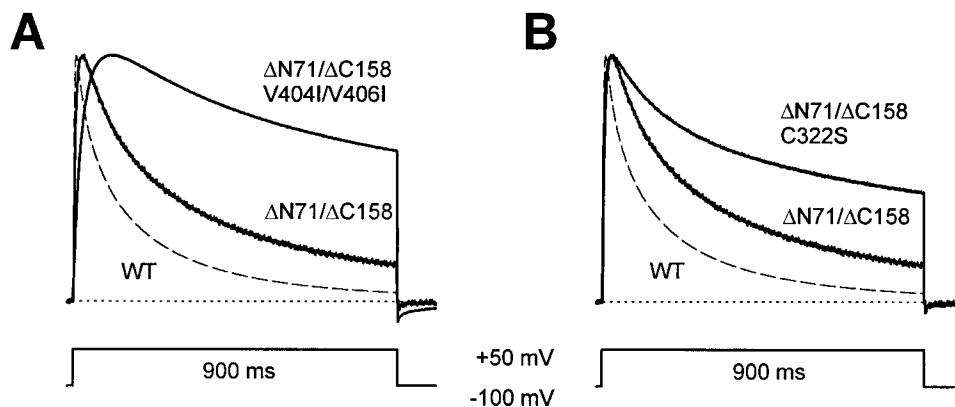ΔN71/ΔC158

WT

900 ms

FIGURE 7. Macroscopic inactivation of Kv4.1 channels in the presence and absence of the cytoplasmic NH$_2$- and COOH-terminal domains. Whole-oocyte currents were elicited by the indicated pulse protocol. All traces are shown normalized. The biophysical properties of the double deletion mutant (ΔN71/ΔC158) were characterized in a previous study (Jerng and Covarrubias, 1997).
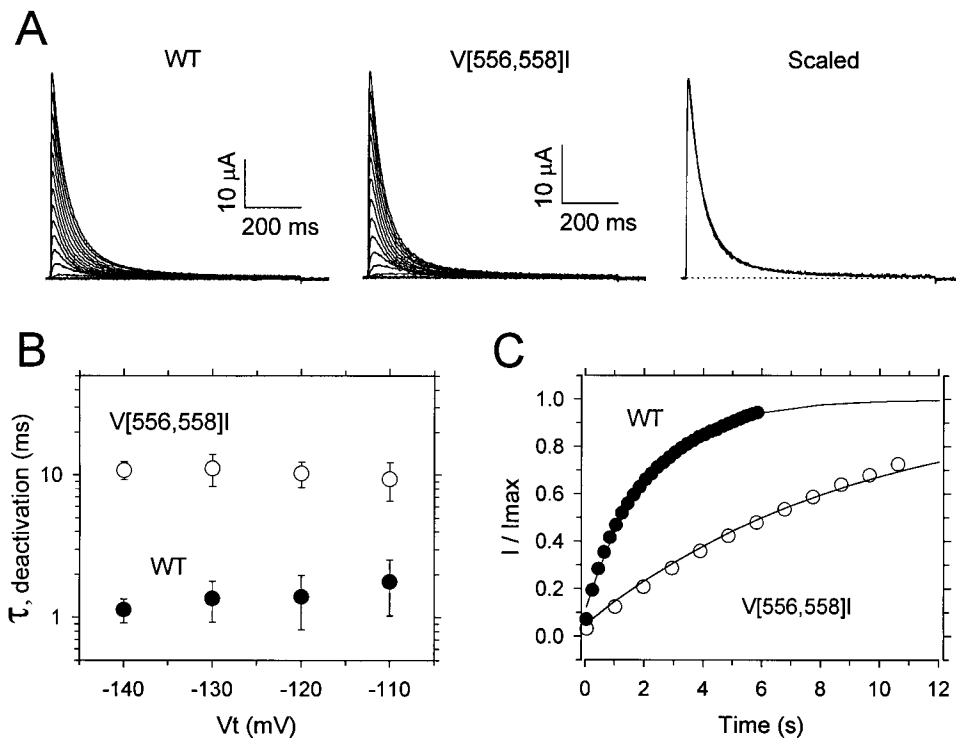
FIGURE 8. Macroscopic Kv1.4 K+ currents expressed in *Xenopus* oocytes. (A) Whole-oocyte currents evoked by 900-ms step depolarizations from a holding potential of −100 mV to test pulses from −80 to +50 mV in 10-mV increments. The interepisode interval in all experiments was 10 and 45 s for wild-type and mutant channels, respectively. (Right) A comparison of normalized wild-type and mutant currents at +50 mV. (B) The effect of membrane potential on the time constant of the tail current relaxations. The experiments were conducted and analyzed as described in Fig. 4. The main difference was that the interpulse interval for the recording of mutant currents was prolonged (30 s). Symbols and bars represent the mean ± SD (wild-type, $n = 5$; mutant, $n = 5$). (C) The time course of recovery from inactivation at −100 mV. The experiment was conducted and analyzed as described in Fig. 2. The time constants of recovery from inactivation (solid lines) were 2 and 12 s for wild-type and mutant channels, respectively.

ble II). Note that V[404,406]I in Kv4.1 channels caused a hyperpolarizing shift of the peak G/V curve and a depolarizing shift of the prepulse inactivation curve (Fig. 3, and Table I).

In addition to the effects on channel gating, the V[556,558]I mutation drastically reduced the sensitivity of the Kv1.4 channels to 4-AP. This property was evaluated by recording two successive current–voltage relations in the absence and presence of 20 mM 4-AP (separated by ∼7 min). Although this protocol is not sufficient to develop steady state use-dependent blockade, in wild-type channels we observed a characteristically faster decay of the current in the presence of 4-AP (the fast time constant of inactivation decreased by two- to threefold) and 66% inhibition of the peak current (Table II). This inhibition is influenced by N-type inactivation and has been previously characterized in detail as an open channel blockade (Yao and Tseng, 1994; Rasmusson et al., 1995). The V[556,558]I mutation eliminated the blockade of the current by 4-AP (Table II). Overall, these results demonstrate that valines in the distal section of S6 in Kv4.1 and Kv1.4 influence channel gating and 4-AP binding, but exert radically different actions on channel inactivation. Clearly, two classes of A-type K+ channels inactivate by distinct mechanisms.

table ii

Properties of Wild-Type and Mutant Kv1.4 Currents*

	Wild type	V[556,558]I
G/V relation		
$V_{0.5}$ (mV)	−60.6 ± 3.0	−48.4 ± 2.1
S (mV)	23.2 ± 0.8	30.1 ± 3.3
	($n = 7$)	($n = 4$)
Prepulse inactivation		
$V_{0.5}$ (mV)	−55.7 ± 1.2	−44.6 ± 2.7
S (mV)	3.4 ± 0.7	3.6 ± 0.5
	($n = 3$)	($n = 3$)
Onset of inactivation		
τ-1 (ms)	47.1 ± 12.9	54.8 ± 20.9
τ-2 (ms)	159 ± 55	233 ± 58
W-1	0.75 ± 0.10	0.86 ± 0.03
W-2	0.24 ± 0.11	0.13 ± 0.02
W-ss	0.02 ± 0.01	0.01 ± 0.01
	($n = 4$)	($n = 5$)
Recovery from inactivation τ (ms)		
	1719 ± 546	9400 ± 809
	($n = 4$)	($n = 3$)
Deactivation τ (ms)	1.1 ± 0.2	10.8 ± 1.6
	($n = 4$)	($n = 3$)
Block by 4-AP percent inhibition	65.9 ± 16.0	0.0 ± 0.2
	($n = 5$)	($n = 3$)

*Analysis, abbreviations, and symbols are as described in Table I.

discussion

Kv4 K$^+$ channels play critical roles in both the central nervous system and the heart. In brain, these channels constitute the somatodendritic subthreshold A-type K$^+$ current that prevents back propagation of action potentials and helps to regulate the frequency of slow repetitive spike firing (Serodio et al., 1996; Hoffman et al., 1997; Johns et al., 1997; Song et al., 1998). In ventricular myocytes, Kv4 channels underlie the Ca-independent A-type outward current known as I$_{to}$ (Dixon et al., 1996; Johns et al., 1997; Yeola and Snyders, 1997). This current helps to shape the early phase of the cardiac action potential. Inactivation gating is crucial for these functions.

To investigate the molecular mechanism underlying inactivation gating of Kv4 K$^+$ channels, we examined the biophysical effects of mutations in the distal section of the S6 region (V[404,406]I and V406I) and the S4–S5 loop (C322S) of Kv4.1. Both regions are putative components of the inner vestibule of the pore (Doyle et al., 1998; Durell et al., 1998). Valines 404 and 406 are conserved in most Kv channels and we hypothesized that they may contribute to the mutually exclusive interaction between 4-AP and inactivation gating in Kv4 K$^+$ channels. C$_{322}$ is a Kv4-specific residue that in conjunction with V404 and V406 may play a key function in the inactivation mechanism. The V[404,406]I and C322S mutations similarly slowed inactivation, deactivation, and inhibited blockade by 4-AP in a manner that is independent of the cytoplasmic NH$_2$- and COOH-terminal domains. Although the effects appeared to be complex, the key to the mechanism of inactivation in Kv4.1 K$^+$ channels was the parallel relation between macroscopic inactivation and deactivation (see below). The specificity and novel nature of these findings is supported by the starkly different effects of homologous mutations in the S6 region of a Kv channel that undergoes N- and C-type inactivation (Kv1.4).

Kv4 K$^+$ Channels Mainly Inactivate from a Preopen Closed State

Our previous study (Jerng and Covarrubias, 1997) and the current data suggest the presence of at least two relatively independent pathways of inactivation at positive membrane potentials in Kv4.1 K$^+$ channels. One is relatively fast ($\tau \sim 15$ ms), contributes to a small percentage of the total decay ($\sim 17\%$), and is affected by both NH$_2$- and COOH-terminal deletions. The other is slow and exhibits two measurable relaxations: intermediate ($\tau \sim 75$ ms) and slow ($\tau \sim 250$ ms); contributing to ~ 35 and $\sim 45\%$ of the total decay, respectively. The S6 and S4–S5 loop mutations characterized in this study drastically affect the more prominent intermediate and

slow processes. Also, slower macroscopic inactivation induced by the mutations was associated with slower current deactivation and a slightly accelerated rate of recovery from inactivation. Thus, we concluded that to enter the dominant inactivated states at depolarized voltages channel closing and inactivation are coupled (i.e., to inactivate, the channel must close). This coupling is disrupted by 4-AP because this agent interacts with the closed channels and slows macroscopic inactivation. Therefore, to explain our observations with Kv4.1 channels, a kinetic model must account for the apparent coupling between inactivation, deactivation, and channel blockade by 4-AP, which constitutes the main experimental constraint on the kinetic analysis. Qualitatively, the simplified Schemes Ia and Ib can explain the main results.

(SCHEME Ia) (SCHEME Ib)
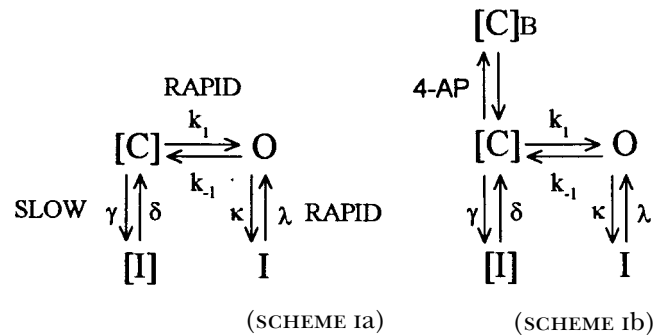
In Schemes Ia and Ib, [C] represents the rapid equilibrium of voltage-dependent state transitions that precede channel opening, and [I] represents an aggregate of inactivated states (transitions outside of the main activation pathway are assumed to be voltage independent). Channels can rapidly reach an inactivated state from the open state (the rapid pathway). However, such a state is unstable ($\lambda > \kappa$). This is consistent with the presence of a small fast component in the decay of the current (see above). Thus, if the equilibrium is shifted toward the closed state (e.g., $k_{-1} > k_1$), the channels may inactivate from a closed state (preferably from that state that precedes channel opening). This pathway may correspond to the slower processes of inactivation. If the C $\leftrightarrow$ O and O $\leftrightarrow$ I equilibria are relatively rapid in Scheme Ia, the slow time constant of inactivation from the preopen closed state can be approximated as $\tau_i \approx (P_c\gamma + \delta)^{-1}$, where P_c is the equilibrium probability of occupying the inactivation permissive preopen closed state [$k_{-1}P_{ro}(k_{-1}P_{ro} + k_{+1})^{-1}$], and P_{ro} is the reopen equilibrium probability [$\lambda(\lambda + \kappa)^{-1}$]. Thus, by changing one rate constant (k_{-1}) in Scheme Ia, it can be seen that channel closing influences inactivation. Because 4-AP mainly blocks closed channels, Scheme Ib shows that inactivation and 4-AP binding are mutually exclusive, as demonstrated
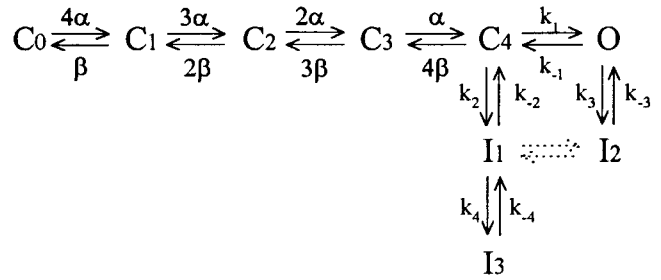
by Campbell et al. (1993b) and Tseng et al. (1996). As for the effects of the mutations, inactivation from the pre-open closed state becomes unfavorable when the C $\leftrightarrow$ O equilibrium in Scheme Ia is shifted toward the open state (e.g., k_{-1} is reduced). Therefore, the macroscopic current decays at a slower rate and 4-AP binding is reduced. This is a likely mechanism because the mutations slowed the closing rate (Figs. 4 and 6). Other important but less significant changes are discussed later assuming an expanded version of Scheme Ia.

A strictly sequential scheme, which assumes inactivation coupled to channel opening (Scheme II), cannot explain the results with Kv4.1 channels. If the C $\leftrightarrow$ O equilibrium is relatively rapid, the time constant of inactivation in Scheme II is approximated as $\tau_i \approx (P_o\kappa + \lambda)^{-1}$ (where P_o is the opening probability in the absence of inactivation; Ayer and Sigworth, 1997). Thus, a shift in the opening equilibrium toward the open state (by simply slowing the closing rate) accelerates macroscopic inactivation (i.e., τ_i decreases). This prediction is opposite of the observations with Kv4.1 channels (i.e., deactivation parallels inactivation). Also, Scheme II with a slower closing rate predicts slower recovery from inactivation because channels revisit the open state when they recover from inactivation. This change is also opposite of the effect of the mutations in Kv4.1, which in fact slightly accelerated the recovery from inactivation. It could be argued that a relatively large simultaneous reduction of both k_{-1} and κ may explain the apparent coupling between channel closing and inactivation. However, such changes in Scheme II also predict a significant increase in the level of the steady state current, which was not observed with the Kv4.1 mutants (and these mutants exhibited only slightly accelerated recovery from inactivation). Scheme II appears more appropriate to describe the results with Kv1.4 channels (see below).

RAPID

$$[C] \underset{k_{-1}}{\overset{k_1}{\rightleftharpoons}} O \underset{\kappa}{\overset{\lambda}{\rightleftharpoons}} \text{SLOW}$$

$$I$$
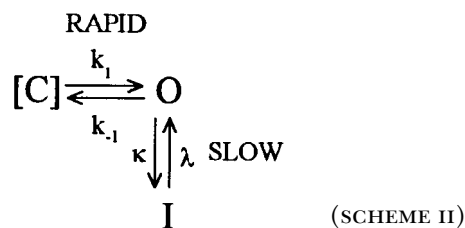
(SCHEME II)

To demonstrate more quantitatively the mechanism described above, we simulated the currents assuming a nine-state time-homogeneous Markov model (Scheme III) as an expanded version of Scheme Ia. This expansion is necessary to account for voltage-dependent gating and sigmoidal activation kinetics. Scheme III can model the main kinetic features of the macroscopic currents at positive voltages (over a range of four orders of magnitude in time) and the tail current at hyperpolarized voltages (Fig. 9).

$$C_0 \underset{\beta}{\overset{4\alpha}{\rightleftharpoons}} C_1 \underset{2\beta}{\overset{3\alpha}{\rightleftharpoons}} C_2 \underset{3\beta}{\overset{2\alpha}{\rightleftharpoons}} C_3 \underset{4\beta}{\overset{\alpha}{\rightleftharpoons}} C_4 \underset{k_{-1}}{\overset{k_1}{\rightleftharpoons}} O$$

$$k_2 \updownarrow k_{-2} \quad k_3 \updownarrow k_{-3}$$

$$I_1 \cdots I_2$$

$$k_4 \updownarrow k_{-4}$$

$$I_3$$

(SCHEME III)

Similar schemes have been previously proposed to describe inactivation gating of A-type K$^+$ channels (Solc and Aldrich, 1990; Zagotta and Aldrich, 1990; Campbell et al., 1993a; Tseng-Crank et al., 1993; Ayer and Sigworth, 1997; Roux et al., 1998). However, in contrast to these models, Scheme III assumes that channel closing is faster than opening ($k_{-1} > k_1$), and that the inactivated state that originates from the open state is unstable ($k_{-3} \geq k_3$). These two assumptions are compatible with single channel recordings showing rapid flickering behavior (Fig. 5). It also assumes, as explained above, that the channels mainly inactivate from the preopen closed state and that this pathway includes at least two inactivated states. Scheme III accounts for the complexity of the macroscopic current at positive voltages. Table III summarizes the sets of parameters that were used to model the wild-type and mutant currents (Fig. 9).

As explained above, the main experimental observation that constrains the kinetic analysis of Kv4.1 inactivation is the apparent parallel relation between the development of current inactivation and deactivation. Three changes of the model's parameters were sufficient to closely reproduce the effects of the mutations. (a) A 19-fold reduction of the closing rate k_{-1}. This change alone significantly slows the tail current and the rising and decaying phases of the macroscopic outward current (Fig. 9, thin line). (b) To account for the slow closed-state inactivation observed with the V[404,406]I mutant, the transition rates governing $C_4 \rightarrow I_1$ (k_2) and $I_1 \rightarrow I_3$ (k_4) were reduced by two- and fivefold, respectively. (c) The inactivation rate k_3 was reduced by $\sim$30% and the reopening rate k_{-3} was approximately doubled because the fast phase of inactivation was also slowed and reduced by the mutations. These changes suggest that the S6 mutations studied here may also modestly affect the process of inactivation that involves the concerted action of the cytoplasmic NH$_2$- and COOH-terminal domains (Jerng and Covarrubias, 1997). It should be noted, however, that the most dramatic kinetic changes induced by the V[404,406]I mutation appear to result from slowing channel closing
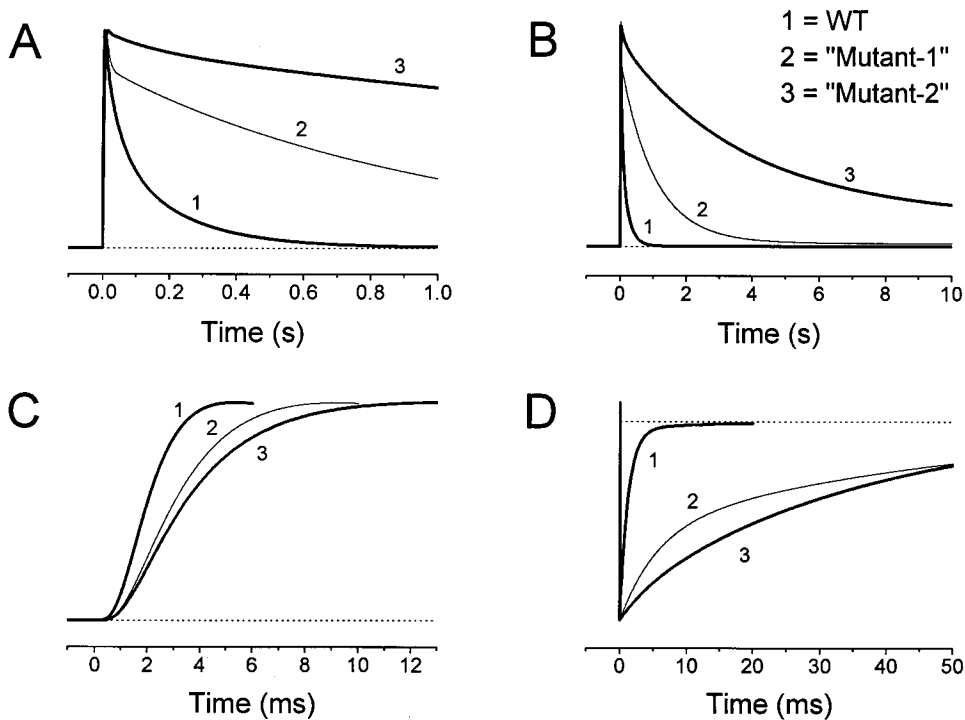
FIGURE 9. Simulated K⁺ currents according to Scheme III. (A) Outward currents generated by assuming a 1-s voltage-step from -100 to $+50$ mV. The parameters of the simulation were as shown in Table III. The key for the calculated traces is shown on the right-hand side of B. To calculate the "Mutant-1" trace, only the closing rate k_{-1} was reduced (39.5 s^{-1}). To calculate the "Mutant-2" trace, the parameters were adjusted to approximate V[404,406]I currents (Table III). The decay of the calculated wild-type (WT) current is well described assuming a sum of three exponential terms: $\tau_1 = 17$ ms (0.2), $\tau_2 = 60$ ms (0.4), and $\tau_3 = 250$ ms (0.4); the sustained level was <0.01 (relative weight of the exponential term in parentheses). These values are consistent with the results of the analysis of Kv4.1 inactivation (Table I). The degree of inactivation of the simulated Mutant-2 current $[I_{(450\ ms)}/I_{peak}]$ is 0.8, which is 10-fold higher than the value calculated from the WT current. These values are also in agreement with observations (see text). (B) Outward currents generated by assuming a 10-s voltage step from -100 to $+50$ mV. (C) The rising phase of the calculated outward currents shown in A. The $T_{50\%}$ of the WT and Mutant-2 traces are 1.8 and 3.2 ms, respectively, and the corresponding activation delays were 1.2 and 1.5 ms (see text). Similar values were measured from the observed currents. (D) Inward tail currents generated by assuming a protocol similar to that described in Fig. 4 ($V_{tail} = -140$ mV). The WT and Mutant-2 currents can also be described assuming exponential relaxations with time constants that agree with the observations (Fig. 4). Dotted lines represent the zero current level.

and closed-state inactivation. The slower inactivation of C322S, on the other hand, was mainly the result of slowing channel closing (k_{-1}) and, to some extent, of slowing k_3 and accelerating k_{-3}. Scheme III also accounted for the kinetics of the tail currents from mutant channels, which exhibited two time constants. The fast and slow relaxations are probably associated with the rapid equilibrium O $\leftrightarrow$ I$_2$ (at the peak of the current ~15% of the mutant channels have entered I$_2$) and channel closing, respectively (Fig. 9). The voltage-dependent activation rate constant α did not seem affected because the activation delay was not significantly different between wild-type and mutant channels (see RESULTS). When β is very small (as expected at depolarized voltages), the activation delay approximates the mean latency to arrive at the open state (Schoppa and Sigworth, 1998).

The V[556,558]I mutation in Kv1.4 channels also slowed current deactivation (Fig. 8). However, by contrast to V[404,406]I in Kv4.1, it had little impact on the time course of macroscopic inactivation but also significantly slowed the recovery from inactivation (Fig. 8,

and Table II). As discussed above, these changes are more consistent with inactivation coupled to channel opening (Scheme II), which is a favored pathway of inactivation of Kv1.4 channels and other A-type K⁺ channels in the *Shaker* family (Hoshi et al., 1990, 1991; Ruppersberg et al., 1991; Tseng-Crank et al., 1993; Baukrowitz and Yellen, 1995; Lee et al., 1996; Ayer and Sigworth, 1997; Roux et al., 1998). Because macroscopic inactivation did not appear accelerated (as predicted earlier for Scheme II when channel closing is slower), it is possible that the V[556,558]I mutation in Kv1.4 might have also modestly reduced the rate of inactivation. Modeling of inactivation coupled to channel opening showed that accelerated macroscopic inactivation caused by a 10-fold slower closing rate can be compensated by a 30% slower rate of inactivation. Altogether, a kinetic model that mainly assumes inactivation coupled to channel opening can explain the results with Kv1.4 channels but fails to account for the apparent coupling between channel closing and the development of inactivation observed with Kv4.1 channels.

Summary and Limitations of the Kinetic Analysis

The initial analysis adopted Scheme Ia to explain inactivation coupled to channel closing and hypothesized that the main effect of the mutations is to slow the closing rate. Thus, to test this hypothesis further, the main goal of the simulations was to determine whether Scheme III (the expanded version of Scheme Ia) can model wild-type and mutant currents in the time domain when $k_{-1} > k_1$ and when k_{-1} is reduced. To evaluate the simulations, we focused our attention on two sets of experiments that examine: (a) currents evoked by short and long depolarizing steps to positive membrane potentials (up to +70 mV), which covered about four orders of magnitude in the time domain (1 ms to 10 s); and (b) tail currents at negative membrane potentials (−140 to −100 mV). The simulations succeeded in simulating the results of these experiments (Fig. 9, and Table III) and revealed that slower closed-state inactivation may also significantly contribute to slower inactivation of macroscopic mutant currents. However, we did not examine in detail the voltage dependence of activation and inactivation. Therefore, there is uncertainty about the complexity of the activation pathway, which may include multiple closed and inactivated states (Zagotta and Aldrich, 1990; Zagotta et al., 1994; Ayer and Sigworth, 1997; Olcese et al., 1997; Klemic et al., 1998; Roux et al., 1998). Nevertheless, at a qualitative level, the same set of parameters (Table III) predicted the observed shifts in the peak G/V relation and the prepulse inactivation curve, and little change in the recovery from inactivation. Also, because of the complexity of the single channel records of wild-type currents, we have not yet obtained more quantitative constraints of the model parameters. To account for the presence of subconductance levels, we have assumed that: (a) the open state in Scheme III represents an aggregate of states with different unitary conductances, and (b) partly and fully open channels can undergo rapid inactivation.

Kv4.1 K⁺ Channels Do Not Undergo N- and C-Type Inactivation

In Kv4.1 channels, the fast component of macroscopic inactivation is eliminated by deletion of the first 31 amino acids at the NH$_2$ terminus and certain COOH-terminal deletions (Pak et al., 1991; Jerng and Covarrubias, 1997). However, additional experimental criteria that are crucial in defining N-type inactivation in *Shaker* K⁺ channels (Choi et al., 1990; Demo and Yellen, 1991; Hoshi et al., 1990; Isacoff et al., 1991) are not satisfied by Kv4.1 K⁺ channels (Jerng and Covarrubias, 1997): (a) internal tetraethylammonium does not compete with a putative inactivation particle; (b) basic residues within the first 40 amino acids at the NH$_2$-terminal domain

table iii
Values of the Simulation Parameters in Scheme III

Parameter*	Wild type	Mutant	Fold change‡
α_0 (s⁻¹)	300	300	0
β_0 (s⁻¹)	5	5	0
V_α (mV)	30	30	0
V_β (mV)	16	16	0
k_1 (s⁻¹)	250	250	0
k_{-1} (s⁻¹)	750	39.5	−19
k_2 (s⁻¹)	21.5	10	−2.1
k_{-2} (s⁻¹)	5	5	0
k_3 (s⁻¹)	75	50	−1.5
k_{-3} (s⁻¹)	90	170	+1.8
k_4 (s⁻¹)	8	1.7	−4.7
k_{-4} (s⁻¹)	0.05	0.05	0

*The rate constants α and β were assumed to depend exponentially on the membrane potential according to these expressions: $\alpha(V) = \alpha_0 \exp(V_m/V_\alpha)$ and $\beta(V) = \beta_0 \exp(-V_m/V_\beta)$. Thus, α increases and β decreases with membrane depolarization. $\alpha_0 = \alpha$ at 0 mV; $\beta_0 = \beta$ at 0 mV; V_m = membrane potential; V_α and V_β are the corresponding slope factors (voltage dependence) of the rate constants. ‡The relative increment (+) or decrement (−) of a parameter.

main are not critical in determining the rate of inactivation; (c) elevated external K⁺ slows recovery from inactivation (in disagreement with the presence of an internal inactivation particle that acts as an open channel blocker); and (d) the S4–S5 loop does not appear to contribute to the docking site of a putative inactivation particle because C322S does not significantly compromise the stability of the inactivated state (for an extended argument, see RESULTS), and other mutations of a highly conserved glutamate in the S4–S5 loop (E325Q and E325D), which disrupt inactivation of *Shaker* channels, in fact accelerated macroscopic inactivation in Kv4.1 (Jerng, 1998).

The removal of fast inactivation by NH$_2$- and COOH-terminal deletions in Kv4.1 channels leaves slower inactivation processes that appear to function independently from the fast process (Jerng and Covarrubias, 1997). Additional results rendered the slow *Shaker* C-type mechanism in Kv4 K⁺ channels also unlikely (Jerng and Covarrubias, 1997): (a) high external tetraethylammonium (96 mM) moderately inhibits the current but does not interfere with inactivation; (b) elevated external K⁺ accelerates recovery from C inactivation (Levy and Deutsch, 1996), but slows recovery from inactivation in Kv4.1; and (c) elevated external K⁺ slows the rate of C-type inactivation (Lopez-Barneo et al., 1993), but accelerates macroscopic Kv4.1 inactivation. C-type inactivation involves residues in the S5–S6 linker and the S6 transmembrane segment (Hoshi et al., 1991; Lopez-Barneo et al., 1993). In particular, mutation of a threonine to valine at position 449 in *Shaker* B

(T449V) nearly eliminates C-type inactivation (Lopez-Barneo et al., 1993). In Kv4 proteins, a valine already exists at the equivalent position. The oxidizing agent chloramine-T accelerates C-type inactivation and induces irreversible current rundown in the NH_2-terminal deleted *Shaker* B channels (Schlief et al., 1996). M448 is implicated as a target for chloramine-T. Although in Kv4.1 channels a methionine occupies the equivalent position, exposure to 1 mM chloramine-T caused no effect on these channels (Jerng, H.H., unpublished observations). Altogether, the data suggest the presence of new components of inactivation gating in Kv4 channels.

A Structural Working Hypothesis of a Novel Component of Inactivation Gating in Kv4 K+ Channels

The external vestibule of Kv channels has been extensively studied and there is a consensus about its structure and function (Aiyar et al., 1995, 1996; Gross and MacKinnon, 1996; Ranganathan et al., 1996; Doyle et al., 1998). The inner vestibule of these channels is, by contrast, more complex and less well understood. Nevertheless, several studies have begun to define the structural components of the inner vestibule of Kv channels (see INTRODUCTION). In particular, it has been demonstrated that components of the inner vestibule (S4–S5 loop and the distal section of S6) undergo conformational changes that can be related to channel gating (Holmgren et al., 1996; Liu et al., 1997). Here, we have characterized a form of inactivation gating in Kv4.1 K+ channels that depends on the coupling between channel closing and inactivation at depolarized membrane potentials (channels must close before they inactivate),

and involves components of the inner vestibule of the pore. The results demonstrated that a Kv4-specific cysteine in the S4–S5 loop (C322) and two valines located in the distal section of S6 (V404 and V406) are important in controlling the inactivation mechanism that is coupled to channel closing. A corollary of this result implies that other residues (or processes) that control channel closing may also influence inactivation, but this remains to be investigated. Because Kv4.1 channels do not exhibit the hallmarks of N- and C-type inactivation (see previous section) and the new observations described here, a novel mechanism of inactivation might be present in these channels. However, the current evidence cannot completely rule out that channel closing at the inner vestibule influences C-type inactivation from partly activated closed states (Olcese et al., 1997), which could involve a P-type component at the external mouth of the pore (De Biasi et al., 1993; Loots and Isacoff, 1998). We suggest the term "V-type" inactivation to indicate that putative components of the inner vestibule affect inactivation gating of Kv4 channels in an unexpected way. In current structural models of the cytoplasmic side of Kv channels, the S4–S5 loop and the distal section of S6 contribute to the inner mouth of the pore (Durell et al., 1998). Thus, in Kv4 channels the inner mouth of the pore (acting as a single gate) may undergo shutter-like conformational changes that sequentially close and inactivate the channel. Closed-state inactivation is also a major gating pathway in slow-inactivating Kv2 channels (Klemic et al., 1998) and the L382I *Shaker* B mutant (Ayer and Sigworth, 1997). However, it is not yet clear whether the V-type component is also present in these channels.

references

Aiyar, J., J.M. Withka, J.P. Rizzi, D.H. Singleton, G.C. Andrews, W. Lin, J. Boyd, D.C. Hanson, M. Simon, B. Dethlefs, and K.G. Chandy. 1995. Topology of the pore-region of K+ channel revealed by the NMR-derived structures of scorpion toxins. *Neuron.* 15:1169–1181.

Aiyar, J., J.P. Rizzi, G.A. Gutman, and K.G. Chandy. 1996. The signature sequence of voltage-gated potassium channels projects into the external vestibule. *J. Biol. Chem.* 271:31013–31016.

Armstrong, C.M., and F. Bezanilla. 1977. Inactivation of the sodium channel. II. Gating current experiments. *J. Gen. Physiol.* 70:567–590.

Ayer, R.K., Jr., and F.J. Sigworth. 1997. Enhanced closed-state inactivation in a mutant *Shaker* K+ channel. *J. Membr. Biol.* 157:215–230.

Baukrowitz, T., and G. Yellen. 1995. Modulation of K+ current by frequency and external [K+]: a tale of two inactivation mechanisms. *Neuron.* 15:951–960.

Campbell, D.L., R.L. Rasmusson, Y. Qu, and H.C. Strauss. 1993a. The calcium-independent transient outward potassium current in isolated ferret right ventricular myocytes: basic characterization and kinetic analysis. *J. Gen. Physiol.* 101:571–601.

Campbell, D.L., Y. Qu, R.L. Rasmusson, and H.C. Strauss. 1993b. The calcium-independent transient outward potassium current in isolated ferret right ventricular myocytes: closed state reverse use-dependent block by 4-aminopyridine. *J. Gen. Physiol.* 101: 603–626.

Chabala, L.D., N. Bakry, and M. Covarrubias. 1993. Low molecular weight poly(A)$^+$ mRNA species encode factors that modulate gating of a non-*Shaker* A-type K$^+$ channel. *J. Gen. Physiol.* 102:713–728.

Choi, K., R.W. Aldrich, and G. Yellen. 1991. Tetraethylammonium blockade distinguishes two inactivation mechanisms in voltage-activated K$^+$ channels. *Proc. Natl. Acad. Sci. USA.* 88:5092–5095.

Covarrubias, M., A. Wei, L. Salkoff, and T.B. Vyas. 1994. Elimination of rapid potassium channel inactivation by phosphorylation of the inactivation gate. *Neuron.* 13:1403–1412.

De Biasi, M., H.A. Hartmann, J.A. Drewe, M. Taglialatela, A.M. Brown, and G.E. Kirsch. 1993. Inactivation determined by a single site in K$^+$ pores. *Pflügers Arch.* 422:354–363.

Demo, S.D., and G. Yellen. 1991. The inactivation gate of the *Shaker* K$^+$ channel behaves like an open-channel blocker. *Neuron.* 7:743–753.

Dixon, J.E., W. Shi, H.S. Wang, C. McDonald, H. Yu, R.S. Wymore, I.S. Cohen, and D. McKinnon. 1996. Role of the Kv4.3 K$^+$ channel in ventricular muscle. A molecular correlate for the transient outward current. *Circ. Res.* 79:659–668.

Doyle, D.A., J.M. Cabral, R.A. Pfuetzner, A. Kuo, J.M. Gulbis, S.L. Cohen, B.T. Chait, and R. MacKinnon. 1998. The structure of the potassium channel: molecular basis of K$^+$ conduction and selectivity. *Science.* 280:69–77.

Durell, S.R., Y. Hao, and H.R. Guy. 1998. Structural models of the transmembrane regions of voltage-gated and other K$^+$ channels in closed, open and inactivated conformations. *J. Struct. Biol.* 121:263–284.

Gomez-Lagunas, F., and C.M. Armstrong. 1995. Inactivation in *Shaker* B K$^+$ channels: a test for the number of inactivating particles on each channel. *Biophys. J.* 68:89–95.

Gross, A., and R. MacKinnon. 1996. Agitoxin footprinting the *Shaker* potassium channel pore. *Neuron.* 16:399–406.

Hoffman, D.A., J.C. Magee, C.M. Colbert, and D. Johnston. 1997. K$^+$ channel regulation of signal propagation in dendrites of hippocampal pyramidal neurons. *Science.* 387:869–875.

Holmgren, M., M.E. Jurman, and G. Yellen. 1996. N-type inactivation and the S4–S5 region of the *Shaker* K$^+$ channel. *J. Gen. Physiol.* 108:195–206.

Hoshi, T., W.N. Zagotta, and R.W. Aldrich. 1990. Biophysical and molecular mechanisms of *Shaker* potassium channel inactivation. *Science.* 250:533–538.

Hoshi, T., W.N. Zagotta, and R.W. Aldrich. 1991. Two types of inactivation in *Shaker* K$^+$ channel: effects of alterations in the carboxyl-terminal region. *Neuron.* 7:547–556.

Isacoff, E.Y., Y.-N. Jan, and L.-N. Jan. 1991. Putative receptor for the cytoplasmic inactivation gate in the *Shaker* K$^+$ channel. *Nature.* 353:86–90.

Jerng, H.H., and M. Covarrubias. 1997. K$^+$ channel inactivation mediated by the concerted action of the cytoplasmic N- and C-terminal domains. *Biophys. J.* 72:163–174.

Jerng, H.H. 1998. Ph.D. Thesis. Thomas Jefferson University, Philadelphia, PA.

Johns, D.C., H.B. Nuss, and E. Marban. 1997. Suppression of neuronal and cardiac outward currents by viral gene transfer of dominant-negative Kv4.2 constructs. *J. Biol. Chem.* 272:31598–31603.

Kirsch, G.E., C.C. Shieh, J.A. Drewe, D.F. Vener, and A.M. Brown. 1993. Segmental exchanges define 4-aminopyridine binding and the inner mouth of K$^+$ pores. *Neuron.* 11:503–512.

Kiss, L., J. LoTurco, and S.J. Korn. 1999. Contribution of the selectivity filter to inactivation in potassium channels. *Biophys. J.* 76:253–263.

Klemic, K.G., C.-C. Shieh, G.E. Kirsch, and S.W. Jones. 1998. Inactivation of Kv2.1 potassium channels. *Biophys. J.* 74:1779–1789.

Lee, T.E., L.H. Philipson, and D.J. Nelson. 1996. N-type inactivation in the mammalian *Shaker* K$^+$ channel Kv1.4. *J. Membr. Biol.* 151:225–235.

Levy, D.I., and C. Deutsch. 1996. Recovery from C-type inactivation is modulated by extracellular potassium. *Biophys. J.* 70:798–805.

Liu, Y., M.E. Jurman, and G. Yellen. 1996. Dynamic rearrangement of the outer mouth of a K$^+$ channel during gating. *Neuron.* 16:859–867.

Liu, Y., M. Holmgren, M.E. Jurman, and G. Yellen. 1997. Gated access to the pore of a voltage-dependent K$^+$ channel. *Neuron.* 19:175–184.

Loots, E., and E.Y. Isacoff. 1998. Protein rearrangements underlying slow inactivation of the *Shaker* K$^+$ channel. *J. Gen. Physiol.* 112:377–390.

Lopez, G.A., Y.-N. Jan, and L.-Y. Jan. 1994. Evidence that the S6 segment of the *Shaker* voltage-gated K$^+$ channel comprises part of the pore. *Nature.* 367:179–182.

Lopez-Barneo, J., T. Hoshi, S.H. Heinemann, and R.W. Aldrich. 1993. Effects of external cations and mutations in the pore region on C-type inactivation of *Shaker* potassium channels. *Receptors Channels.* 1:61–71.

MacKinnon, R., R.W. Aldrich, and A.W. Lee. 1993. Functional stoichiometry of *Shaker* potassium channel inactivation. *Science.* 262:757–759.

McCormack, K., M.A. Tanouye, L.E. Iverson, J.W. Lin, M. Ramaswami, T. McCormack, J.T. Campanelli, M.K. Mathew, and B. Rudy. 1991. A role for hydrophobic residues in the voltage-dependent gating of *Shaker* K$^+$ channels. *Proc. Natl. Acad. Sci. USA.* 88:2931–2935.

McCormack, K., L. Lin, and F.J. Sigworth. 1993. Substitution of a hydrophobic residue alters the conformational stability of *Shaker* K$^+$ channels during gating and assembly. *Biophys. J.* 65:1740–1748.

Murrell-Lagnado, R.D., and R.W. Aldrich. 1993. Interactions of the amino terminal domains of *Shaker* K$^+$ channels with a pore blocking site studied with synthetic peptides. *J. Gen. Physiol.* 102:949–975.

Ogielska, E.M., W.N. Zagotta, T. Hoshi, S.H. Heinemann, J. Haab, and R.W. Aldrich. 1995. Cooperative subunit interaction in C-type inactivation of K$^+$ channels. *Biophys. J.* 69:2449–2457.

Olcese, R., R. Latorre, L. Toro, F. Bezanilla, and E. Stefani. 1997. Correlation between charge movement and ionic current during slow inactivation in *Shaker* K$^+$ channels. *J. Gen. Physiol.* 110:579–589.

Pak, M.D., K. Baker, M. Covarrubias, A. Butler, A. Ratcliffe, and L. Salkoff. 1991. mShal, a subfamily of A-type K$^+$ channel cloned from mammalian brain. *Proc. Natl. Acad. Sci. USA.* 88:4386–4390.

Panyi, G., Z. Sheng, L. Tu, and C. Deutsch. 1995. C-type inactivation of a voltage-gated K$^+$ channel occurs by a cooperative mechanism. *Biophys. J.* 69:896–903.

Pardo, L.A., S.H. Heinemann, H. Terlau, U. Ludewig, C. Lorra, O. Pongs, and W. Stühmer. 1992. Extracellular K$^+$ specifically modulates a rat brain K$^+$ channel. *Proc. Natl. Acad. Sci. USA.* 89:2466–2470.

Ranganathan, R., J.H. Lewis, and R. MacKinnon. 1996. Spatial localization of the K$^+$ channel selectivity filter by mutant cycle-based structure analysis. *Neuron.* 16:131–139.

Rasmusson, R.L., M.J. Morales, R.C. Catellino, Y. Zhang, D.L. Campbell, and H.C. Strauss. 1995. C-type inactivation controls recovery in a fast inactivating K$^+$ channel (Kv1.4) expressed in *Xenopus* oocytes. *J. Physiol.* 489:709–721.

Rettig, J., F. Wunder, M. Stocker, R. Lichtinghagen, F. Mastiaux, S. Beckh, W. Kues, P. Pedarzani, K.H. Schroeter, J.P. Ruppesberg, et al. 1992. Characterization of a Shaw-related potassium channel family in rat brain. *EMBO (Eur. Mol. Biol. Organ.) J.* 11:2473–2488.

Roux, M.J., R. Olcese, L. Toro, F. Bezanilla, and E. Stefani. 1998. Fast inactivation in *Shaker* K$^+$ channels: properties of ionic and gating currents. *J. Gen. Physiol.* 111:625–638.

Ruppersberg, J.P., R. Frank, O. Pongs, and M. Stocker. 1991.

Cloned neuronal $I_k(A)$ channels reopen during recovery from inactivation. *Nature.* 353:657–660.

Shieh, C.-C., and G.E. Kirsch. 1994. Mutational analysis of ion conduction and drug binding sites in the inner mouth of voltage-gated K⁺ channels. *Biophys. J.* 67:2316–2325.

Schlief, T., R. Schonherr, and S.H. Heinemann. 1996. Modification of C-type inactivating *Shaker* potassium channels by chloramine-T. *Pflügers Arch.* 431:483–493.

Schoppa, N.E., and F.J. Sigworth. 1998. Activation of *Shaker* potassium channels: I. Characterization of voltage-dependent transitions. *J. Gen. Physiol.* 111:271–294.

Serodio, P., E. Vega-Saenz de Miera, and B. Rudy. 1996. Cloning of a novel component of A-type K⁺ channels operating at subthreshold potentials with unique expression in heart and brain. *J. Neurophysiol.* 75:2174–2179.

Slesinger, P.A., Y.-N. Jan, and L.-Y. Jan. 1993. The S4–S5 loop contributes to the ion selective pore of potassium channels. *Neuron.* 11:739–749.

Smith, P.L., T. Baukrowitz, and G. Yellen. 1996. The inward rectification mechanism of HERG cardiac potassium channel. *Nature.* 379:833–836.

Solc, C.K., and R.W. Aldrich. 1990. Gating of non-*Shaker* A-type potassium channels in larval *Drosophila* neurons. *J. Gen. Physiol.* 96:135–165.

Song, W.-J., T. Tkatch, G. Baranauskas, N. Ichinohe, S.T. Kitai, and D.J. Surmeier. 1998. Somatodendritic depolarization-activated potassium currents in rat neostriatal cholinergic interneurons are predominantly of the A-type and attributable to coexpression of Kv4.2 and Kv4.1 subunits. *J. Neurosci.* 18:3124–3137.

Starkus, J.G., L. Kuschel, M.D. Reyner, and S.H. Heinemann. 1997. Ion conduction through C-type inactivated *Shaker* channels. *J. Gen. Physiol.* 110:539–550.

Taglialatela, M., M.S. Champagne, J.A. Drewe, and A.M. Brown. 1994. Comparison of H5, S6, and H5-S6 exchanges on pore properties of voltage-dependent K⁺ channels. *J. Biol. Chem.* 269:13867–13873.

Tseng-Crank, J., J.-A. Yao, M.F. Berman, and G.-N. Tseng. 1993. Functional role of the NH₂-terminal cytoplasmic domain of mammalian A-type K channel. *J. Gen. Physiol.* 102:1057–1084.

Tseng, G.-N., M. Jiang, and J.-A. Yao. 1996. Reverse use dependence of Kv4.2 blockade by 4-aminopyridine. *J. Pharmacol. Exp. Ther.* 279:865–876.

Yao, J.-A., and G.-N. Tseng. 1994. Modulation of 4-AP block of mammalian A-type K channel clone by channel gating and membrane potential. *Biophys. J.* 67:130–142.

Yeola, S.W., and D.J. Snyders. 1997. Electrophysiological and pharmacological correspondence between Kv4.2 current and rat cardiac transient outward current. *Cardiovasc. Res.* 33:540–547.

Zagotta, W.N., and R.W. Aldrich. 1990. Voltage-dependent gating of *Shaker* A-type potassium channels in *Drosophila* muscle. *J. Gen. Physiol.* 95:29–60.

Zagotta, W.N., T. Hoshi, J. Dittman, and R.W. Aldrich. 1994. *Shaker* potassium channel gating. II: Transitions in the activation pathway. *J. Gen. Physiol.* 103:279–319.